



National Library
of Canada

Acquisitions and
Bibliographic Services Branch

395 Wellington Street
Ottawa, Ontario
K1A 0N4

Bibliothèque nationale
du Canada

Direction des acquisitions et
des services bibliographiques

395, rue Wellington
Ottawa (Ontario)
K1A 0N4

Your file *Votre référence*

Our file *Notre référence*

NOTICE

The quality of this microform is heavily dependent upon the quality of the original thesis submitted for microfilming. Every effort has been made to ensure the highest quality of reproduction possible.

If pages are missing, contact the university which granted the degree.

Some pages may have indistinct print especially if the original pages were typed with a poor typewriter ribbon or if the university sent us an inferior photocopy.

Reproduction in full or in part of this microform is governed by the Canadian Copyright Act, R.S.C. 1970, c. C-30, and subsequent amendments.

AVIS

La qualité de cette microforme dépend grandement de la qualité de la thèse soumise au microfilmage. Nous avons tout fait pour assurer une qualité supérieure de reproduction.

S'il manque des pages, veuillez communiquer avec l'université qui a conféré le grade.

La qualité d'impression de certaines pages peut laisser à désirer, surtout si les pages originales ont été dactylographiées à l'aide d'un ruban usé ou si l'université nous a fait parvenir une photocopie de qualité inférieure.

La reproduction, même partielle, de cette microforme est soumise à la Loi canadienne sur le droit d'auteur, SRC 1970, c. C-30, et ses amendements subséquents.

Rate dependent response of graphite/epoxy in transverse shear

Sylvain Riendeau
Mechanical Engineering
McGill University, Montreal

February 1995

A thesis submitted to the Faculty of Graduate Studies and Research
in partial fulfilment of the requirements of the degree of Master.

© Sylvain Riendeau 1995



National Library
of Canada

Acquisitions and
Bibliographic Services Branch

395 Wellington Street
Ottawa, Ontario
K1A 0N4

Bibliothèque nationale
du Canada

Direction des acquisitions et
des services bibliographiques

395, rue Wellington
Ottawa (Ontario)
K1A 0N4

Your file *Votre référence*

Our file *Notre référence*

THE AUTHOR HAS GRANTED AN IRREVOCABLE NON-EXCLUSIVE LICENCE ALLOWING THE NATIONAL LIBRARY OF CANADA TO REPRODUCE, LOAN, DISTRIBUTE OR SELL COPIES OF HIS/HER THESIS BY ANY MEANS AND IN ANY FORM OR FORMAT, MAKING THIS THESIS AVAILABLE TO INTERESTED PERSONS.

L'AUTEUR A ACCORDE UNE LICENCE IRREVOCABLE ET NON EXCLUSIVE PERMETTANT A LA BIBLIOTHEQUE NATIONALE DU CANADA DE REPRODUIRE, PRETER, DISTRIBUER OU VENDRE DES COPIES DE SA THESE DE QUELQUE MANIERE ET SOUS QUELQUE FORME QUE CE SOIT POUR METTRE DES EXEMPLAIRES DE CETTE THESE A LA DISPOSITION DES PERSONNE INTERESSEES.

THE AUTHOR RETAINS OWNERSHIP OF THE COPYRIGHT IN HIS/HER THESIS. NEITHER THE THESIS NOR SUBSTANTIAL EXTRACTS FROM IT MAY BE PRINTED OR OTHERWISE REPRODUCED WITHOUT HIS/HER PERMISSION.

L'AUTEUR CONSERVE LA PROPRIETE DU DROIT D'AUTEUR QUI PROTEGE SA THESE. NI LA THESE NI DES EXTRAITS SUBSTANTIELS DE CELLE-CI NE DOIVENT ETRE IMPRIMES OU AUTREMENT REPRODUITS SANS SON AUTORISATION.

ISBN 0-612-05472-1

Canada

Acknowledgment

I would like first of all to thank my supervisor James Nemes for his help throughout my thesis. I would also like to thank all the people who helped me or supported me during my work: George Tewfik, Fernand Picard and his team, Larry Lessard, Nicolas Thomas, Robert Jackson, Yannick, Hamid Eskandari, Mahmood Shokrieh, Gilles Bérubé, Michael J. Worswick, Jean-François Milette, Patrick Lizotte, Phil White, Eric Speciel, Ann-Louise Lock, Farid Hassani, and finally my family, my girlfriend and all the people I forgot.

Abstract

The use of fiber reinforced plastic composites in critical applications has increased dramatically in recent years. To take full advantage of the benefits of these materials, it is essential to be able to predict their behavior under impact. The continuum damage model by Nemes and Randles attempts to answer that need. For a complete formulation, the rate dependence of the material under the different modes of damage has to be quantified. Experiments, where the modes of damage are isolated from each other are therefore needed.

A punching experiment was chosen to isolate the transverse shear response of the composites. The tests were conducted on a 24 ply graphite/epoxy AS4/3501-6 quasi-isotropic lay-up over a wide range of loading rates. Low and medium rate experiments are performed using a hydraulic testing machine with a specially designed punch shear fixture to obtain load versus displacement results. High rate experiments (in the order of 10^3) are performed using a punch shear version of the split Hopkinson bar apparatus, which was developed as part of this project.

For both kinds of tests, load versus displacement curves were obtained at different loading rates. The specimens were x-rayed to evaluate the damage inflicted to the specimen. Optical microscopy of sectioned samples of partially punched specimens was used to construct a sequence of the damage process.

Cracking initiates in the shear zone of the specimen side contacted by the punch bar. This is followed by delamination in the lower part of the plug. Finally, after significant rotation of the material, tensile failure occurs. The plug can then be pushed out.

The maximum load reached for different loading rates does not show any rate dependence. It is postulated that the peak value would depend on the fiber tensile properties which are rate-independent for graphite. Some rate-dependence is observed during the loading of the specimens. It is thought to reflect the matrix cracking response. The rate dependence for the transverse shear properties is considered to be significant enough to be included in impact analyses.

Résumé

Les matériaux composites ont acquis, au fil des ans, une utilisation répandue. Il est primordial de pouvoir prédire leur comportement sous impact. Le modèle d'endommagement continu de Nemes et Randles pourrait répondre à ce besoin. Pour une formulation complète, l'influence de la vitesse de chargement sur le matériau, soumis à différents modes d'endommagement, doit être quantifié. Des méthodes expérimentales où les modes d'endommagements sont isolés les uns des autres sont requises.

Un test de poinçonnement a été choisi pour isoler la réponse en cisaillement transversal des composites. Les tests ont été effectués sur des stratifiés de 24 plis de graphite/époxyde. La séquence d'empilement a été choisie afin d'obtenir un comportement quasi-isotrope. Les tests à basses et moyennes vitesses de chargement sont effectués à l'aide d'une machine d'essais hydraulique standard (MTS) équipée d'un appareil de fixation de l'échantillon. Les tests à hautes vitesses de déformation (ordre de grandeur de 10^3) sont effectués grâce à une version en cisaillement de la méthode de barres d'Hopkinson. Les équipements furent conçus et fabriqués dans le cadre de ce mémoire.

Pour les différents tests, des courbes de la force en fonction du déplacement ont été obtenues. Les spécimens ont été radiographiés pour évaluer l'endommagement. L'observation au microscope optique a également été utilisée pour déterminer les modes de progression de l'endommagement.

Les fissures débutent dans la zone de cisaillement du côté du poinçon. Le délaminage de la partie inférieure de la zone poinçonnée suit. Finalement, après la rotation du matériel, une rupture en tension des fibres se produit. La zone poinçonnée peut alors être éjectée du spécimen.

Le chargement maximum atteint ne démontre pas de dépendance envers la vitesse de chargement. Il est supposé que cette valeur est liée aux propriétés en tension des fibres de graphite qui sont indépendantes de la vitesse de chargement. Une dépendance est cependant observée durant le chargement du spécimen. Ce comportement refléterait l'effet de la fissuration de la matrice. Cette dépendance envers la vitesse de chargement, pour les propriétés en cisaillement transversal, est considérée assez importante pour être incluse dans toute analyse d'impact.

Table of Contents

ACKNOWLEDGMENT	I
ABSTRACT	II
RÉSUMÉ	III
TABLE OF CONTENTS	IV
LIST OF FIGURES	V
LIST OF TABLES	VII
LIST OF SYMBOLS	VIII
1-INTRODUCTION	1
2-BIBLIOGRAPHICAL REVIEW	3
3-MOTIVATION	14
4-EXPERIMENTAL CONFIGURATION	18
4.1-HOPKINSON BARS	18
4.1.1-Theory	18
4.1.2-Composite lab facilities	23
4.1.3-Design of the components	25
The bars	25
The supports	27
The specimen holder	28
The slide	28
The gas gun	29
The momentum trap	32
The Alignment	32
Electronic equipment	32
Strain pulses acquisition	33
Calibration	34
Speed detector	35
4.2-STATIC TESTS	37
5-MATERIAL	39

6-TEST PROCEDURES	40
7-RESULTS	42
7.1-RESULTS COMPARISON	47
8-SPECIMEN INSPECTION	50
8.1-X-RAY	50
8.2-VISUAL INSPECTION	53
9-MODES OF FAILURE	56
10-RECOMMENDED FURTHER RESEARCH	57
11-CONCLUSION	58
12-REFERENCES	59
13-APPENDIX	61

List of Figures

FIGURE 1.1 RANGE OF STRAIN RATES	1
FIGURE 2.1 STRESS VS STRAIN FOR GRAPHITE/EPOXY IN COMPRESSION	3
FIGURE 2.2 ULTIMATE COMPRESSIVE STRESS VS STRAIN RATE	4
FIGURE 2.3 MAXIMUM NORMAL STRESS VARIATION WITH ANGLE-PLY FIBER ORIENTATION FOR GFRP IN TENSION	5
FIGURE 2.4 TENSILE STRESS/STRAIN CURVE FOR CFRP	5
FIGURE 2.5 DETAIL OF INPUT AND OUTPUT PRESSURE BAR LOADING INTERFACES USED FOR SHEAR TESTING AND THE TWO LOADING CONFIGURATIONS	6
FIGURE 2.6 SHEAR STRESS VERSUS SHEAR STRAIN FOR TRANSVERSE SHEAR	7
FIGURE 2.7 SIMPLE OVERLAP SPECIMEN	8
FIGURE 2.8 FAILURE STRENGTHS AND YIELD STRESSES VERSUS STRAIN RATES	9
FIGURE 2.9 LOAD DISPLACEMENT CURVES FOR A PUNCHING TEST; MEAN PUNCH SPEED A: 2.5×10^{-7} B: 2.5×10^{-6} C: 2.5×10^{-4} D:3 E:11 F:18	11
FIGURE 2.10 LAMINATE DEFORMATION	12
FIGURE 3.1 THRESHOLD SURFACE FOR THE ONSET OF DAMAGE	16
FIGURE 4.1 DIFFERENT HOPKINSON BAR APPARATUS	19

FIGURE 4.2 LAGRANGIAN DIAGRAM	21
FIGURE 4.3 SCHEMATIC PUNCH AND DIE	21
FIGURE 4.4 SPLIT HOPKINSON BAR SYSTEM	25
FIGURE 4.5 SUPPORT	27
FIGURE 4.6 SPECIMEN HOLDER	28
FIGURE 4.7 THE SLIDE	29
FIGURE 4.8 GAS GUN SECTION	30
FIGURE 4.9 WHEATSTONE BRIDGE	33
FIGURE 4.10 INCIDENT BAR READING	34
FIGURE 4.11 TRANSMITTED BAR READING	34
FIGURE 4.12 FORCE HISTORY	34
FIGURE 4.13 DISPLACEMENT HISTORY	34
FIGURE 4.14 MCGILL UNIVERSITY HOPKINSON BAR SYSTEM A) BARS B) NITROGEN TANK C) OSCILLOSCOPE D) GAS GUN AND SLIDE	36
FIGURE 4.15 STATIC FIXTURE	37
FIGURE 4.16 FIXTURE RESPONSE (CURVE) AND MODEL (LINEAR)	38
FIGURE 7.1 PUNCHING SPEED = 0.001M/S	42
FIGURE 7.2 PUNCHING SPEED = 0.01M/S	43
FIGURE 7.3 PUNCHING SPEED =0.1 M/S	44
FIGURE 7.4 PUNCHING SPEED =4.2 M/S	45
FIGURE 7.5 PUNCHING SPEED = 6 M/S	45
FIGURE 7.6 COMPARISON OF LOWER STRIKER VELOCITY TESTS (8 AND 10 M/S) TO A STANDARD ONE	46
FIGURE 7.7 EFFECT OF BAD PUNCH SURFACE	47
FIGURE 7.8 1 AND 10 SEC TESTS	48
FIGURE 7.9 HIGH SPEED PUNCHING	49
FIGURE 7.10 THREE DIFFERENT MODES	49
FIGURE 8.1 LOW PUNCHING LOAD	50
FIGURE 8.2 ALMOST PUNCHED	50
FIGURE 8.3 PUNCHED SPECIMEN	51
FIGURE 8.4 DIE APPLIED ON THE PLUG	51
FIGURE 8.5 HOLDERS EFFECTS	51
FIGURE 8.6 21kN LOAD	53
FIGURE 8.7 31kN LOAD	54
FIGURE 8.8 MAXIMUM LOAD REACHED	54
FIGURE 8.9 COMPLETELY PUNCHED SPECIMEN	54
FIGURE 8.10 PLUG BEING PUSHED OUT	55

LIST OF TABLES

TABLE 2.1 COMPARISON OF MECHANICAL CHARACTERISTICS OF T300/5208 AT DIFFERENT STRAIN RATES _9

List of Symbols

A_i	Area of surface I
α_i	Damage parameter
C_0	Longitudinal wave speed
d_i	Distance to the Threshold surface
ΔE	Difference in voltage
ΔL	Barrel length
Δu	Displacement of face 1 relatively to face 2
$\Delta u'$	Corrected displacement
E	Young's modulus
E_{ij}	Young's modulus in the i direction
ϵ_i	Incident strain pulse
ϵ_R	Reflected strain pulse
ϵ_t	Transmitted strain pulse
F	Force on the specimen
F_1	Force in the incident bar
F_2	Force in the transmitted bar
G_{ij}	Shear modulus
J_i	Stain gage number i
K	Constant
M_s	Mass of the sabot
M_b	Mass of the bar
P	Pressure
R_i	Resistance number i
t	time
u_i	Displacement in the i direction
ν_{12}	Poisson's ratio
V_i	Speed of the striker
V_i	Damage vector in the i direction
V_s	In-plane damage vector

1-Introduction

The use of composite materials has increased dramatically in the last decades. They are used in many applications ranging from recreational equipment to the high technology aerospace field. Their biggest advantages are their strength and stiffness-to-weight ratio. It makes them a natural choice for applications where the weight is critical as in the aerospace industry. Other properties of these materials may make them advantageous for specific applications. For example, the electrical properties of fiberglass make them a common choice for applications where a rigid structure that does not conduct electrical current is needed.

In general, composite material usage has not yet reached its full potential. One of the major causes of that is the lack of complete understanding of the behavior of the material. The study of composites is still relatively recent. Many fields have not been thoroughly studied yet. Among those, is the behavior under impact, which plays a big role in many applications.

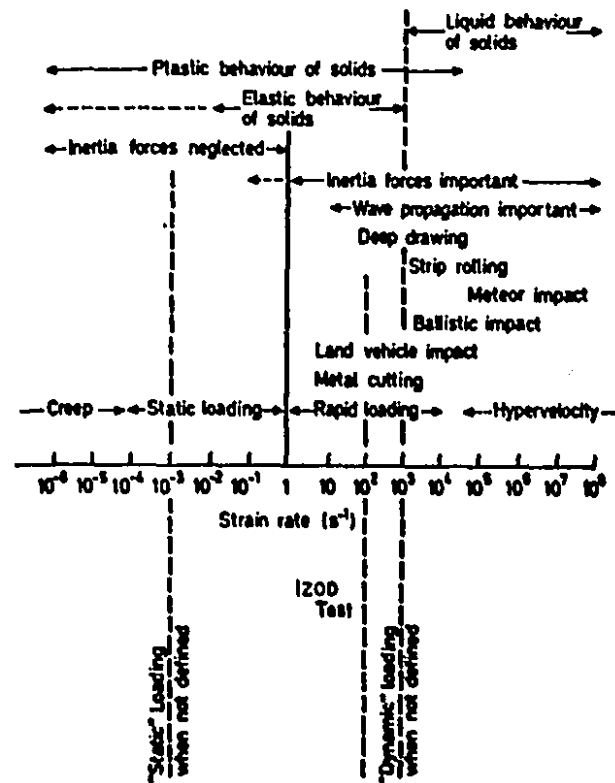


Figure 1.1 Range of strain rates [1]

A better understanding of the rate-dependent behavior is needed to use composite materials in applications involving severe dynamic loading. Different kinds of loading can be represented by the strain rates they produce. Figure 1.1 [1] shows a variety of strain rates found.

The typical impact experiment involves impact of a steel sphere onto a composite plate. It produces complex states of stress that make it difficult to understand the constitutive behavior of the material. Tests in which one type of loading is isolated are needed. A punching experiment is used here to characterize the transverse shear behavior of fiber reinforced plastic laminates at different loading speeds. For this investigation, a special version of the split Hopkinson bar apparatus has been designed and built to measure the high rate response. The slower tests are performed on a standard material testing system (MTS) with a special fixture.

In the following section, previous studies on the effect of the strain rates on the different mechanical properties of composites materials will be presented. This work will then be brought into perspective by presenting briefly Nemes and Randles continuum damage constitutive model. The design and development of the experimental apparatus will be presented followed by the measured results. Finally, inspection of specimens using x-rays and optical microscopy are used to help formulate the failure modes.

2-Bibliographical review

The field of fiber reinforced laminated composites under impact is extensive. This review will concentrate on the properties of composites under different loading rates and on experimental investigations that relate to what is done in the scope of this work.

In most investigations similar test procedures are used. In that, slow and medium rate tests are done on a MTS or an INSTRON testing machine. The high rate tests are performed on a specially designed apparatus, such as the Hopkinson bar apparatus. This is the technique used in this research and it will be introduced in a later section of this text.

One of the easiest tests to perform is the measurement of the material response in compression. The Hopkinson apparatus needed then is kept to its simplest form: two bars with the specimen sandwiched between them. The compression properties of laminates vary only slightly with the strain rates. Figure 2.1 [2] shows stress/strain curves for Graphite/Epoxy (CFRP) at different strain rates and temperatures. The material, AS4/3501-6, is the same that was used in this research. The curves, for three different strain rates at room temperature, show that both Young's modulus, as determined from the slope of the curve, and the maximum stress increase with increasing strain rate.

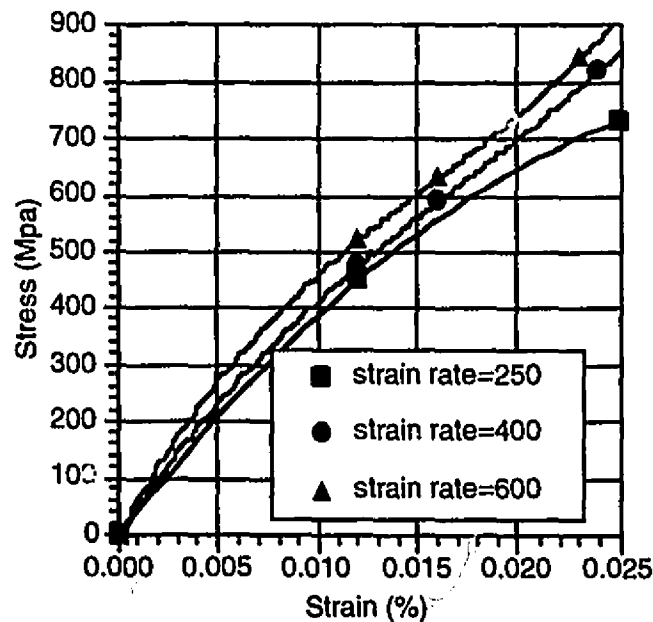


Figure 2.1 Stress vs strain for graphite/epoxy in compression [adapted from 2]

In compression testing, the rate effect is similar for glass fiber (GFRP). Figure 2.2 [3] shows the maximum compressive stress for different types of GFRP. The maximum stress depends on the resin type and the fiber volume fraction. The reinforced fibre treatment does not have much effect.

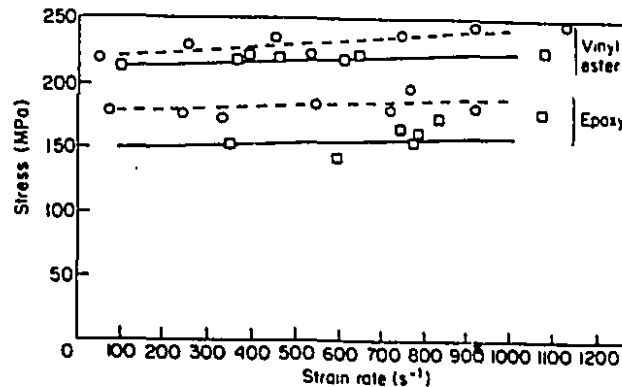


Figure 2.2 Ultimate compressive stress vs strain rate
 □ Glass fiber treatment A
 ○ Glass fiber treatment B [3]

These results, for tests in the fiber direction for unidirectional or bi-directional composites, indicate that, for most FRP, the strength and modulus increase only slightly with strain rates.

A second group of important tests investigates the tensile properties. The equipment needed is more complex and different types of Hopkinson bar apparatus have been used. The most significant point to remember is that glass fiber laminates do not behave like carbon fiber. The behavior of GFRP (Glass/Epoxy) varies greatly with strain rates while the behavior of CFRP is not significantly affected by it. Tests with angle ply GFRP showed that glass fibers were rate sensitive. In fact, they contribute more to the rate sensitivity than the matrix. Figure 2.3 [4] shows the difference between static and dynamic strength for different fiber orientations. Figure 2.4 [5] shows the variation in stress/strain curves for unidirectional CFRP (Hyfil-Torayca-130-S/R7H). The curves, representing different strain rates, are offset for clarity.

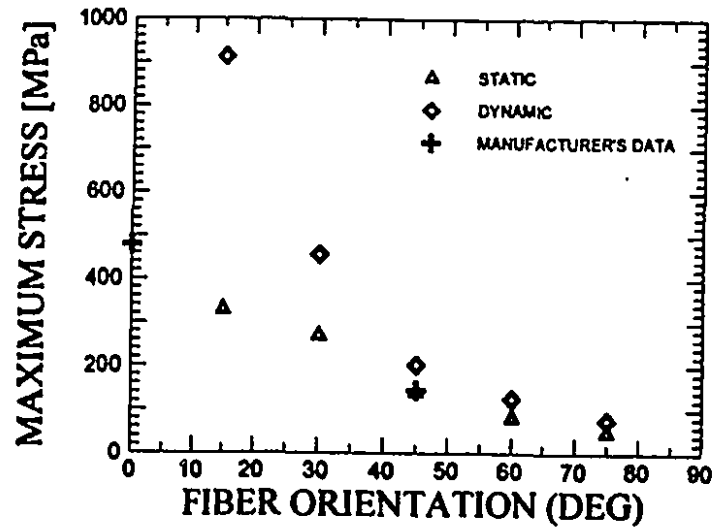


Figure 2.3 Maximum normal stress variation with angle-ply fiber orientation for GFRP in tension[4]

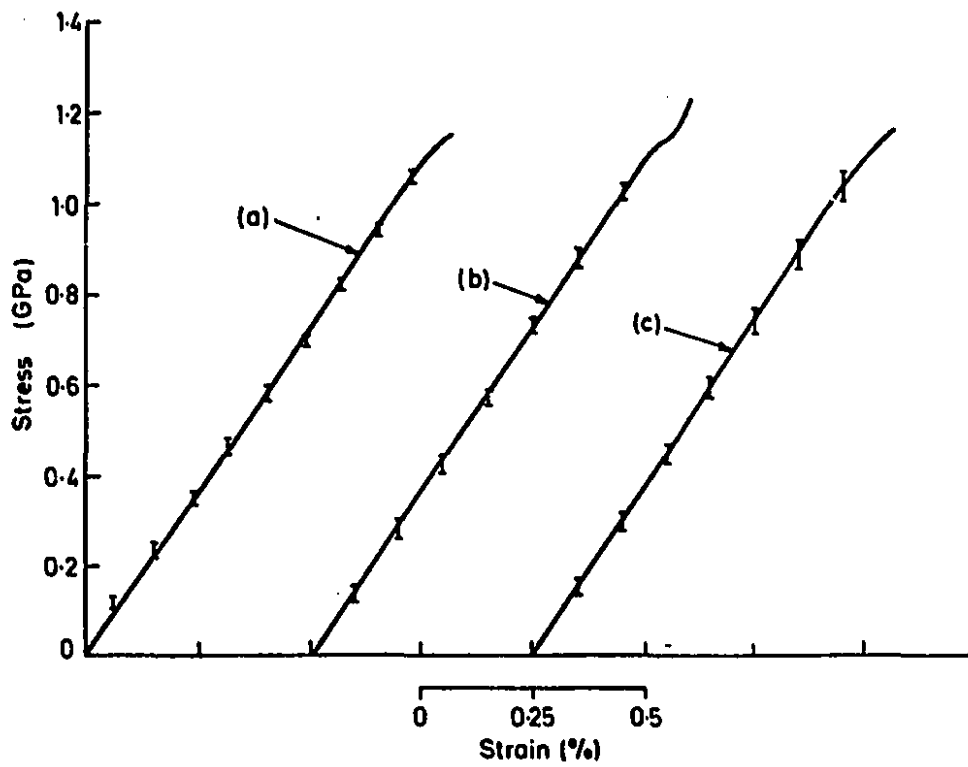


Figure 2.4 Tensile stress/strain curve for CFRP [5]

Another important parameter to investigate is rate-dependence of the shear properties of the materials. The special nature of laminates will dictate two different shear properties to examine. The first one is the interlaminar shear. It consists of the resistance to shear in the plane of the plies. The second one is the transverse shear which acts in the plane perpendicular to the plies. Different results have been obtained in this area. Some research teams have come to opposite conclusions. The testing configuration and the specimens used in each experiment varied. For the purpose of this report, some of the methods used and their results will be presented.

One test that can be performed in such an investigation is the three point bend test. Werner and Dharan [6] used this test in conjunction with Hopkinson bars. Figure 2.5 shows the configuration for the interlaminar and the transverse shear. Graphite-epoxy was used for the specimens.

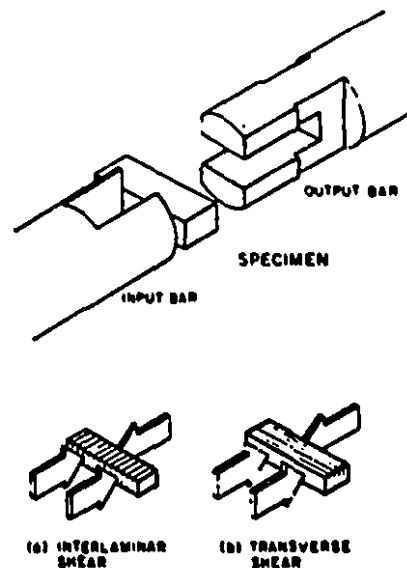


Figure 2.5 Detail of input and output pressure bar loading interfaces used for shear testing and the two loading configurations [6]

There was considerable scatter in the obtained data. Within that scatter, it still appears that the interlaminar shear stress response is relatively constant for all strain rates. In transverse shear loading, increasing strain rates resulted in a decrease in the shear strength and softening. Figure 2.6 [6] shows the results for transverse shear.

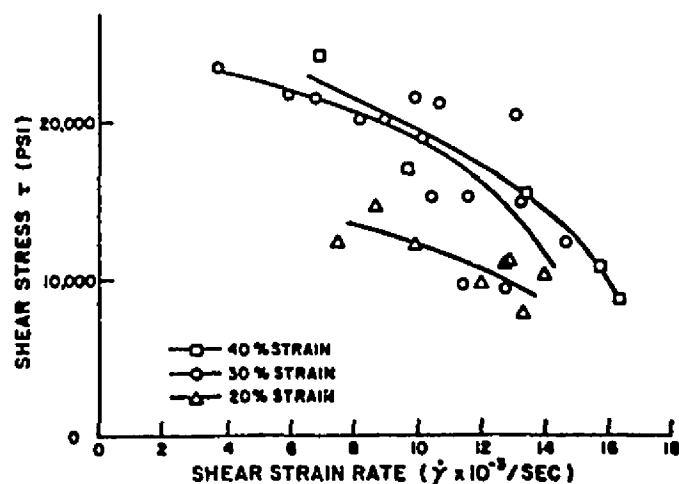


Figure 2.6 Shear stress versus shear strain for transverse shear [6]

For interlaminar shear strength, two other ways to investigate this property will be briefly introduced. The first method confirms the results found by Werner And Dahran but the second one contradicts them, since an increase in stiffness and strength is found with a rise in strain rate.

Bouette, Cazeneuve and Oytana [7] developed an overlap specimen that applies an interlaminar shear on the laminate. A schematic illustration of the specimen is presented in Figure 2.7. The specimen has been designed in conjunction with a finite element analysis. The analysis was used to find an optimum configuration where the stress field is mostly interlaminar shear.

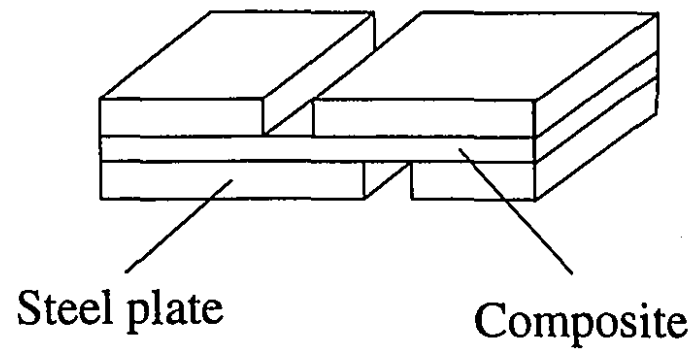


Figure 2.7 Simple overlap specimen [adapted from 7]

This experiment showed once again that the mechanical characteristics of interlaminar shear do not vary with strain rate. The material used in this investigation was unidirectional graphite epoxy T300/5208. Table 2.1 shows the values obtained.

	Low strain rate (10^{-3} s^{-1})	Intermediate strain rate (1 s^{-1})	High strain rate (10^3 s^{-1})
Shear Modulus: G_{13} (GPa)	5.6 ± 0.1	5.6 ± 0.1	5.5 ± 0.3
Shear Strength: S_{13} rupture (MPa)	74 ± 3	71 ± 2	73 ± 4

Table 2.1 Comparison of mechanical characteristics of Graphite-Epoxy T300/5208 at different strain rates [7]

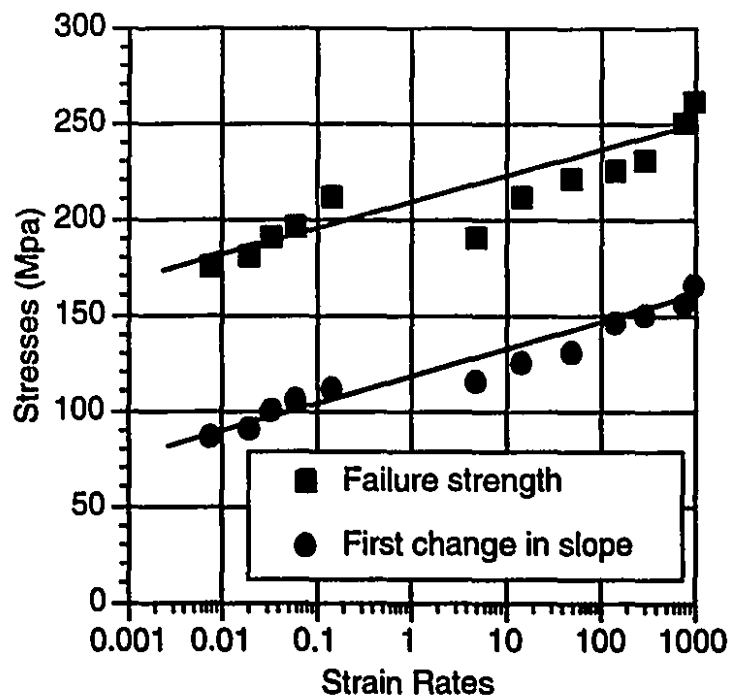


Figure 2.8 Failure strengths and yield shear stresses versus strain rates [8]

Lataillade, Delaet and Collombet [8] showed that the mechanical parameters related to interlaminar shear loading increase in a logarithmic law with low, medium and high strain rates. They used a uniaxial tensile test on symmetrical $[\pm 45]$ Eglass/epoxy crossply laminates. This technique generates a preponderant interlaminar shear loading within each ply of the laminate. Figure 2.8 shows the failure strengths and the first change in slope stresses versus strain rates.

An alternative method to investigate transverse shear is by punching a specimen. Harding [9] did so on woven fiber glass material. He used both polyester and epoxy based matrix. Both matrices gave similar results.

It is difficult in punching experiments to relate the forces and displacements measured to the actual stresses and strains. This is due to the fact that the actual gage length is different from the radial clearance between the punch bar and the die tube. If the same type of experiment is performed on metal the actual deformed zone can be found with micro-hardness tests as was done by Dowling [20]. The zones that undergo large plastic deformation will show a change in the hardness of the material. After the test, measuring the hardness distribution will give an approximate gage length. From this, the stresses and strains can be found from the obtained data. Unfortunately the same process cannot be applied to composites. The zone can only be approximated by post-test observation. In this study, only the force versus displacement results will be presented. The stresses vs strains curves would have similar trends, but are difficult to quantify.

Figure 2.9 [9] shows the load versus displacement curves for woven glass/polyester material. The properties greatly increase with punching speed. This gives an opposite result from the one obtained with the three point bend test of Werner and Dahran [6], although for a different material.

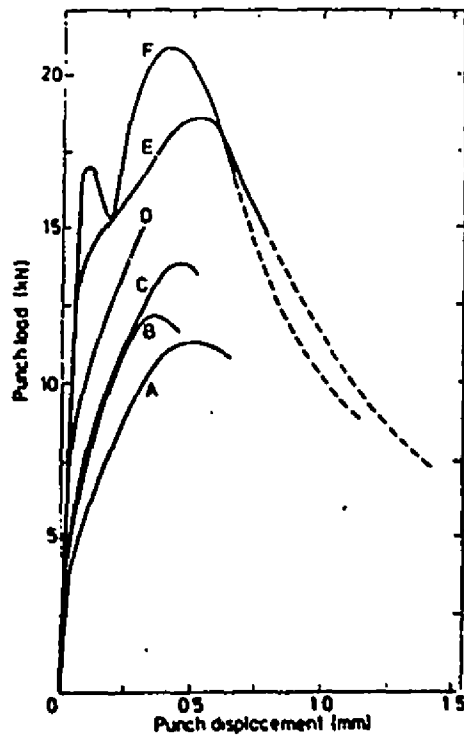


Figure 2.9 Load displacement curves for a punching test; mean punch speed
 A: $2.5 \cdot 10^{-7}$ B: $2.5 \cdot 10^{-6}$ C: $2.5 \cdot 10^{-4}$ D:3 E:11 F:18 [9]

These values are the only one found in the literature for the punching of composites. Some problems were reported by Harding including: low accuracy in measuring the displacement and large scatter in the results. The dashed lines represent extrapolation of results. The two peaks behavior for the fastest test was found in this study. This behavior will be discussed in a further section.

Further more, these tests were only performed on GFRP. This present research focuses on CFRP. Most of the problems faced by Harding were solved in this study. It is also interesting to note that the difference in behavior mentioned previously for tension is also present in punching shear. This fact will be brought in perspective in a later section of this report.

Finally, S.-W. R. Lee and C. T. Sun have performed an investigation on the dynamic penetration of graphite/epoxy (AS4/3501-6) laminates impacted by a blunt-ended projectile. These results are related to what is being done here. In their research, an attempt was made to use the static punching results to predict what will happen when a blunt-ended projectile hits a composite plate

The static punching configuration used in the experiment of Lee and Sun differs from a traditional punching experiment. In that, the gap between the punch and the die is large enough that significant bending of the plate is present. Figure 2.10 [11] shows a cross-sectional view of the laminate deformation.

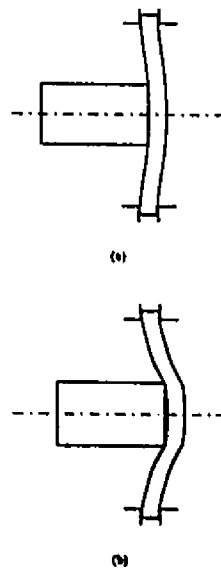


Figure 2.10 laminate deformation [11]

For the same type of lay-up as the one used in this thesis, but for a 33% thicker laminate, the maximum load obtained was approximately half that found here. The difference is attributed to these bending effects.

Three types of testing configurations were used including two different lay-ups and two different spans for the specimens. This gives an indication of how bending affects the loads and the displacements. The presence of significant bending will result in large displacements.

To confirm this assumption, the theory of plates and shells was used to approximate the displacements caused by the load at the first peak. In the calculations, the modulus of the material was approximated by the engineering properties calculated from the laminate flexural matrix.

The ratio of bending deformation to total deformation was found to vary from 40% to close to 100% depending on the test configuration. Thinner specimens with longer spans deform more in bending than thick short ones.

When no bending effects are present, the maximum loads are much higher as is found in this research.

3- Motivation

This research is part of work being done to develop a continuum damage model for composite materials. This model was first introduced by Randles and Nemes in 1992 [12].

In their approach, the evolution equations are taken to be completely phenomenological, that is, no attempt is made to employ a micromechanical model of a growing crack. Due to the complexity of the damage process in composite materials, micromechanical models that accurately describe the evolution are not available at present time. In this model, the evolution equations are taken to be a function of the current state of damage, some overstress above a threshold, and material properties controlling evolution rates. Writing the evolution equations in this form leads to an overall rate-dependent, or time-dependent, material response through the damage process. The material investigated is considered to be transversely isotropic. This is obtained by using a composite with balanced [0/+60] or [0,90,+45] lay-ups.

The matrix damage is characterized by the vector $V=(V_1, V_2, V_3)$ where the direction 1 is perpendicular to the plane of the laminate. The value of V , the damage magnitude, represents the fractional reduction of certain elastic properties of the material. The V_1 component represents the damage induced by delamination. The microcracking damage is represented by a combination of V_2 and V_3 . This damage is assumed to occur in a randomly distributed fashion both spatially and by orientation of normals in the 2,3-plane such that the degraded material properties are left transversely isotropic. It can be concluded that the property degradation depends only on the magnitude of the in-plane components of the damage vector.

$$V_s = \sqrt{V_2^2 + V_3^2} \quad (3.1)$$

The following simple damage dependence of the properties is assumed:

$$\begin{aligned}
 E_{11} &= (1 - V_1^2) E_{11}^0 \\
 E_{22} &= (1 - \alpha_1 V_s^2) E_{22}^0 \\
 G_{12} &= (1 - V_1^2) (1 - \alpha_2 V_s^2) G_{12}^0 \\
 \nu_{12} &= (1 - V_1^2) (1 - \alpha_3 V_s^2) \nu_{12}^0 \\
 \nu_{23} &= (1 - \alpha_4 V_s^2) \nu_{23}^0
 \end{aligned}
 \tag{3.2}$$

Where the superscript 0 denotes virgin properties and the fractions $0 < \alpha < 1$ are included to prevent complete loss of material integrity as the saturation state $V \mapsto 1$ is reached. Integrity may remain due to unbroken reinforcing fibers in the 2,3 plane.

Rate dependency is introduced into the continuum damage model process by way of damage evolution. Both the V_1 and V_s types of damage are assumed to be governed by a threshold of the form:

$$\begin{aligned}
 F(\sigma, f(V)) &< 0 \quad \text{for no damage growth} \\
 &> 0 \quad \text{for damage growth}
 \end{aligned}$$

Where F is a scalar threshold function, σ is the current stress tensor and f is an array of current threshold parameters, which is a function of V . A graphic representation of the threshold surface is shown in figure 3.1.

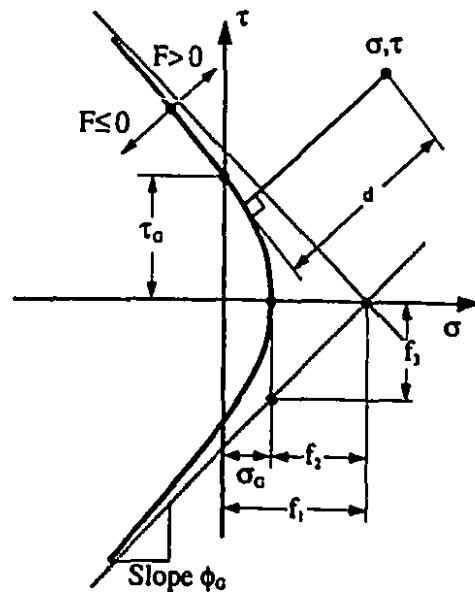


Figure 3.1 Threshold surface for the onset of damage [12]

The evolution equations for the damage are required to complete this model constitutive description. For the V_1 damage, it is postulated that the material damage derivative takes the form:

$$\frac{dV_1}{dt} = F_1 (d_1 V_1) \quad (3.3)$$

Where d_1 is the shortest distance from an exterior stress point to the threshold surface $F=0$. An equivalent relation is postulated for V_S .

These equations can be integrated into a computer code to solve dynamic problems. There are many parameters included in the model formulation, which must be evaluated experimentally. Tests are chosen to separate the effect of the different damage modes or components of stress.

One of these experiments is the punch shear experiments performed here. In this configuration the transverse shear stress is the dominant loading mode. The parameters related to transverse damage can then be evaluated by comparison of measured results with those obtained from finite-element analysis of the experimental configuration. Through an iterative process, the assumed functional forms and material parameters can be chosen such that good agreement is obtained. By choosing a quasi-isotropic configuration, the problem is then reduced to an axisymmetric one. A preliminary investigation using finite element analysis was performed by Thomas [13]. The problem was modeled with axisymmetric elements on ABAQUS [21], a finite elements software, using a simplified version of the continuum damage model. Reasonably good results were obtained. In a later stage of this program this analysis will be performed again to find the parameters matching the experimental values.

4-Experimental configuration

The punching test was performed using two distinct apparatus. The quasi-static tests were done on a MTS machine while the high-rate ones were done on a Hopkinson bar system. The same interface punch/die was used in both cases. The punch diameter is $9.47 \text{ mm} \pm 0.01 \text{ mm}$. The die's inside diameter is $9.53 \text{ mm} \pm 0.01$ while its outside diameter is $12.70 \pm 0.01 \text{ mm}$. The radial clearance between the punch and the die therefore is $0.03 \pm 0.02 \text{ mm}$. The material used for the punch and the die is tool steel O1 (ASTM A681). It was not quenched.

Special care was given on keeping the die and the punch in good condition. The edges were kept at a constant sharpness between the tests to insure constant results. In the same way, the roundness of the punch outside diameter was regularly checked. Finally, both of the end surfaces had to be carefully machined to ensure flatness and perpendicularity with the bar.

In the following section, the Hopkinson bar principle and testing facilities will be introduced in detail. Then, the static equipment will be briefly presented, followed by a discussion of some special considerations on the use of the fixture.

4.1-Hopkinson bars

4.1.1-Theory

For the determination of the high-rate shear properties, a split Hopkinson bar apparatus was selected. It is the most widely used experimental configuration for high strain-rate measurement and was the obvious choice for this research. The development of the Hopkinson bar apparatus was done as part of this research since no comparable apparatus existed at McGill University.

The basic principle behind the Hopkinson bars is that it is possible to determine the stresses, the strains and the displacements occurring at the end of a bar by measuring the

deformation somewhere else in the bar. To do so it is necessary that the elastic waves going through the bar travel in an undisturbed manner. As the waves travel at the velocity of sound in that material, the information recorded will be delayed in time. A long thin bar ($L/d > 20$) is needed to have one dimensional propagation.

The Hopkinson bar got its name from its developer, who in 1914 recognized that, as long as the pressure bar remains elastic, the displacements in the pressure bar are directly related to the stresses and that the length of the wave in the bar was related to the duration of the impact through the velocity of sound in the bar. A few decades later, Kolsky introduced the split Hopkinson pressure bar technique (also called Kolsky bars). In this technique, which is the most widely used, the specimen is sandwiched between two pressure bars. The use of strain gages to measure the strain on the surface of the bars was introduced in the beginning of the 1960's. Since that time, the technological progress in electronics brought improvement in data acquisition equipment. The digital oscilloscope is one of the examples that make these experiments easier.

There are many kinds of Hopkinson bars apparatus. Figure 4.1 [14] shows examples of test configurations possible for different types of testing, namely compression, shear and tension.

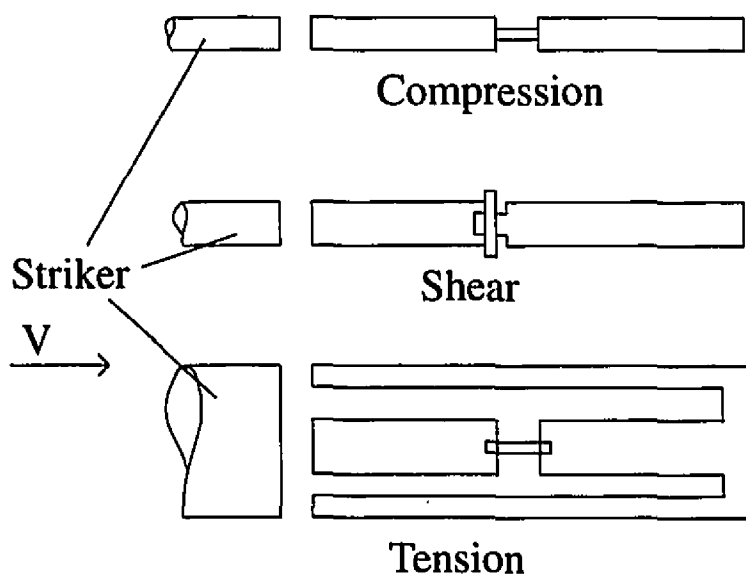


Figure 4.1 Different Hopkinson bar apparatus [Adapted from 14]

In this research, a split Hopkinson bar was used with the interface designed for a punching test. It is closely related, in the way it works, with the widely documented compression apparatus. The mathematics is more complex but is based on the same principles.

The experiment only lasts a few hundreds of microseconds and goes as follow. A striker bar is accelerated to a desired velocity by a nitrogen gas gun. It hits the incident bar producing a compressive wave. The compressive wave travels down the bar at the longitudinal wave speed of the material ($C_0=(E/\rho)^{1/2}$) and passes through the strain gages. This triggers the oscilloscope which begins recording the strain gages readings. Meanwhile, another compressive wave travels backward in the striker; when it reaches the end of the bar it reflects back as a tensile wave, which causes the striker to bounce back at the moment the tensile wave gets to the incident bar. This also stops the compressive wave in the incident bar, producing a duration that is twice the wave transit time in the striker. When the compressive wave reaches the specimen, a portion of the wave is transmitted and a portion is reflected. This is due to the mismatch between the two materials. The transmitted portion through the specimen is again reflected and transmitted at the interface of the specimen and transmitted bar. Since the wave transit time in the short specimen is small compared to the total duration of the test, many wave reflections can take place back and forth in the specimen, producing a quasi-equilibrium condition. At the sample, part of the wave is transmitted to the second pressure bar (transmitted bar) and part bounces back (incident bar). Both portions of the wave propagate down the length of the bars where they will be recorded by the strain gages. At the end of the transmitted bar, a momentum trap will capture the wave and dissipate the energy. A Lagrangian diagram, Figure 4.2, shows the evolution in time of the waves.

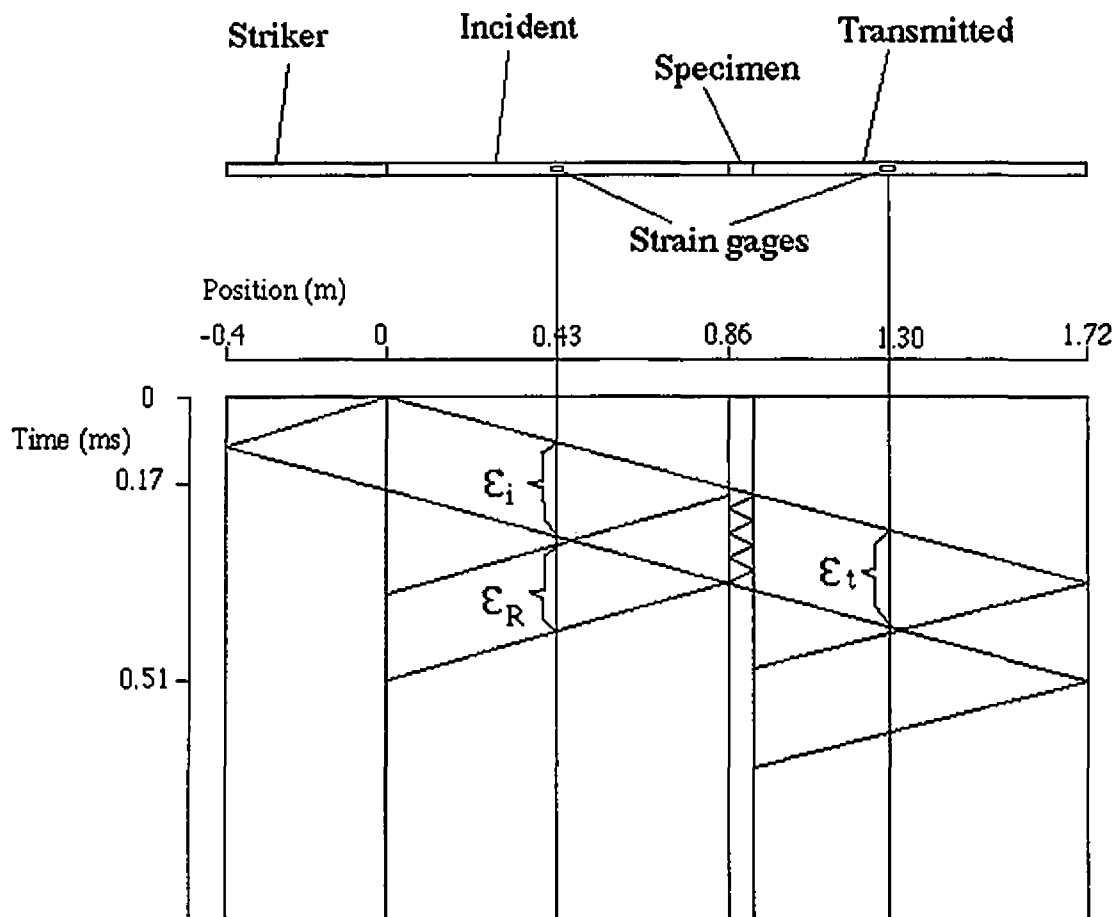


Figure 4.2 Lagrangian diagram

Figure 4.3 shows a schematic representation of the specimen interface for punching split Hopkinson bars. The basic equations will be developed from this.

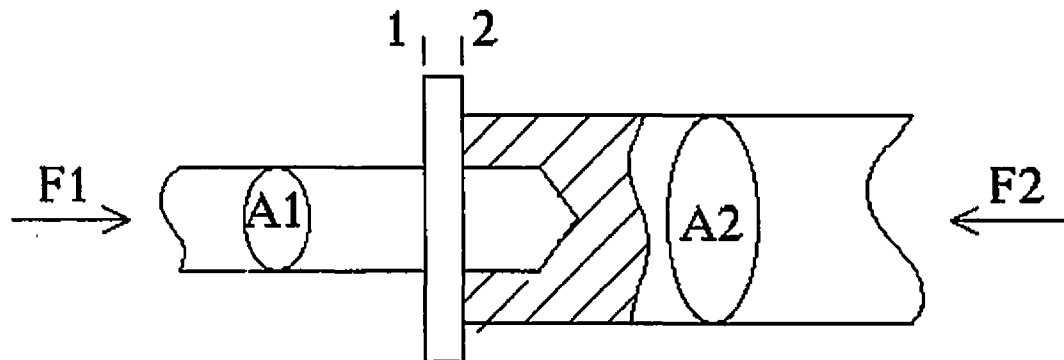


Figure 4.3 Schematic punch and die

U_1 and U_2 refer to the displacement at the end of the bars. Tensile strains are taken as positive.

$$u_1 = \int_0^t C_0 \varepsilon_1 dt$$

$$u_2 = \int_0^t C_0 \varepsilon_2 dt$$
(4.1)

Where C_0 is the longitudinal wave speed of the material and ε_1 and ε_2 are the strains at the interfaces. ε_1 is composed of the incident, ε_i , and the reflected, ε_R , wave pulses while ε_2 is only composed of the transmitted pulse, ε_t . Doing the substitution, the displacement of the punch relatively to the die is given by:

$$\Delta u = u_1 - u_2 = C_0 \int_0^t (\varepsilon_i - \varepsilon_R - \varepsilon_t) dt$$
(4.2)

The forces at the ends of the selected regions are:

$$F_1 = EA_1(\varepsilon_i + \varepsilon_R)$$

$$F_2 = EA_2\varepsilon_t$$
(4.3)

It is assumed that $F_1 = F_2 = F$, so equating the last two equations:

$$A_1(\varepsilon_i + \varepsilon_R) = A_2\varepsilon_t$$

$$\varepsilon_i = \frac{A_2}{A_1} \varepsilon_t - \varepsilon_R$$
(4.4)

Substituting equation (4.4) into equation (4.2)

$$\Delta u = C_0 \int_0^t \left(\epsilon_t \left(\frac{A_2}{A_1} - 1 \right) - 2 \epsilon_R \right) dt \quad (4.5)$$

The force is given by the equation

$$F = EA_2 \epsilon_t \quad (4.6)$$

The pulse magnitude can be related to the striker velocity by conservation of momentum.

The relation is:

$$2 \epsilon_t C_0 = V_i \quad (4.7)$$

Using the equations (4.5) and (4.6) on the test data will give a force versus time and a displacement versus time record. They can be combined to produce a force/displacement graph.

4.1.2-Composite lab facilities

Prior to this research, no previous Hopkinson bar apparatus existed in the mechanical Engineering department of McGill University. Existing Hopkinson bars installations, were visited.

A tensile Hopkinson bar exists at Carleton University (Ontario), in the department of Mechanical and Aerospace Engineering. In addition, the Defense Research Establishment of Val-Cartier has several compression Hopkinson bar apparatus. These facilities were visited to gain a better understanding of the apparatus prior to beginning design.

The basic design consideration for the system were:

- Performance;
- Laboratory restrictions;
- Cost;
- Safety.

Each of these is addressed below.

1- Performance

The material to be tested is a 24 -ply graphite/Epoxy laminate. The pulse magnitude and duration have to be sufficient to completely punch through the specimen. Further more, they have to be able to vary. Different striker lengths and speeds have to be available.

2-Laboratory restrictions

The punching split Hopkinson bars have to be installed on an existing optical table. This table is fixed firmly to the floor. It provides a nice flat surface to which every thing will be attached. Further more for safety reasons, the striker had to be shot in the wall direction.

3-Cost

The major cost in the apparatus is the data acquisition, namely the digital oscilloscope. It was bought with the help of a NSERC grant. The cost of the rest of the equipment can vary greatly upon the design choices made. The costs were kept to their minimal values without influencing the performance.

4-Safety

There are high velocity projectiles and pressure vessels involved in Hopkinson bar experiments. In both the design of the facilities and in the test procedures, total safety of the people present during the tests must be considered.

Figure 4.4 shows a schematic representation of the Split Hopkinson bars apparatus built at McGill University.

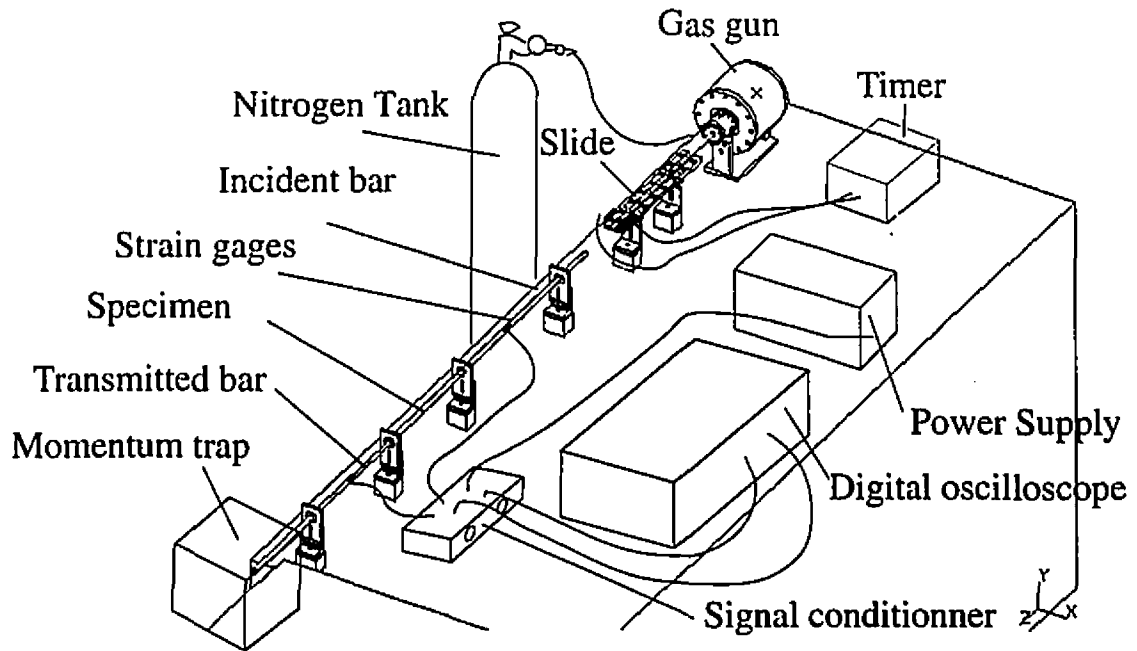


Figure 4.4 Split Hopkinson bar system

4.1.3-Design of the components

The bars

The lengths of the bars were chosen to fit the table.

The incident bar is 0.864 m (34 inches)

The transmitted bar is 0.762 m (30 inches)

Two different strikers were machined

The long striker is 0.406 m (16 inches)

The short striker is 0.203 m (8 inches)

The lengths correspond respectively to the longest pulse the bars can take without superposition and to the smallest bar the gas gun can shoot.

The material was chosen to be tool steel O1. It comes in drill rods of 0.91m (3 feet). The tolerance on the diameter is ± 0.01 mm (± 0.0005 inches), which is sufficient for this use. Machining a rod to this precision would have been costly. Buying it already centerless ground at the plant resulted in significant cost savings. One bar cost approximately 20\$ instead of several hundred. There was no thermal treatment applied on the bars. Thermal treatments would have changed the dimensions considerably. Without heat treatment, though, the yield stress is much lower than what it could have been. The magnitude of the incident pulse must therefore be limited to a lower value to keep the bars in the elastic range, but it is still sufficient for this application. The striker speed must be limited to 19 m/s. If, in the future, the apparatus has to be used to test tougher material, a new set of bars can easily be manufactured.

The diameter to length ratio respects the one-dimensional wave propagation constraint. It is respectively 90.7 and 60.0 for the incident and transmitted bars when the lower limit is evaluated to be 20 [15].

The supports

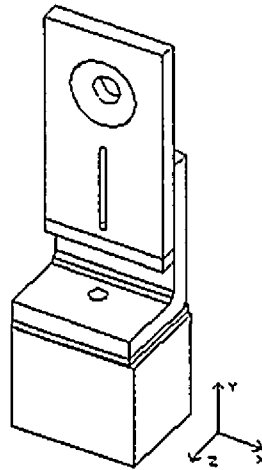


Figure 4.5 Support

The supports (figure 4.5) were designed to take advantage of existing magnets that were used with the optical table. The supports therefore require no permanent fixture to the table. The strength of the magnet is sufficient to keep everything in place. When the bars are well aligned, the only force on the support, besides the gravity forces, is the friction between the bar and the bushings. There is no moment nor forces that will cause the support to release. A Plexiglass spacer had to be installed between the support and the magnet for isolation. The magnetic field was deviated through the support causing a loss in restraint forces.

The only adjustment on the support is the height of the bar (y axis). There is no way to adjust the x rotation. Care must be taken in drilling the bushings to have the hole perpendicular to the magnet top surface. All the other useful degrees of freedom can be adjusted by moving the magnet.

The bushings were made from delran. This plastic does not have a friction coefficient as low as Teflon but is less expensive and easier to machine. It has been chosen for all bushings and for the sabot in the gas gun.

Once every thing is well aligned, the bar slides easily in the supports. Strong friction is a sign that the alignment is not perfect.

The specimen holder

The specimen holder (figure 4.6) consists of a modified support. The specimen is mostly held by the punch and the die. Screws are supporting the specimen against the gravity. The two sides are there only to protect in case some part of the specimen would fly out. They should not touch the specimen .

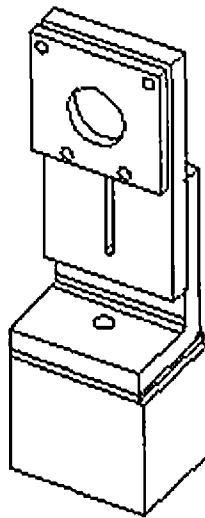


Figure 4.6 Specimen holder

The slide

A slide (Figure 4.7) was built to guide the striker from the gun to the incident bar. This ensures that the striker bar axis is perpendicular to the plane of the specimen. Further more it supports the bar on the vertical axis balancing for the gravity. The slide is made of a thin plate with a v groove. This groove is covered with thin Plexiglass plates that permit easy sliding of the bar. The alignment of the slide is controlled in a similar way as the supports.

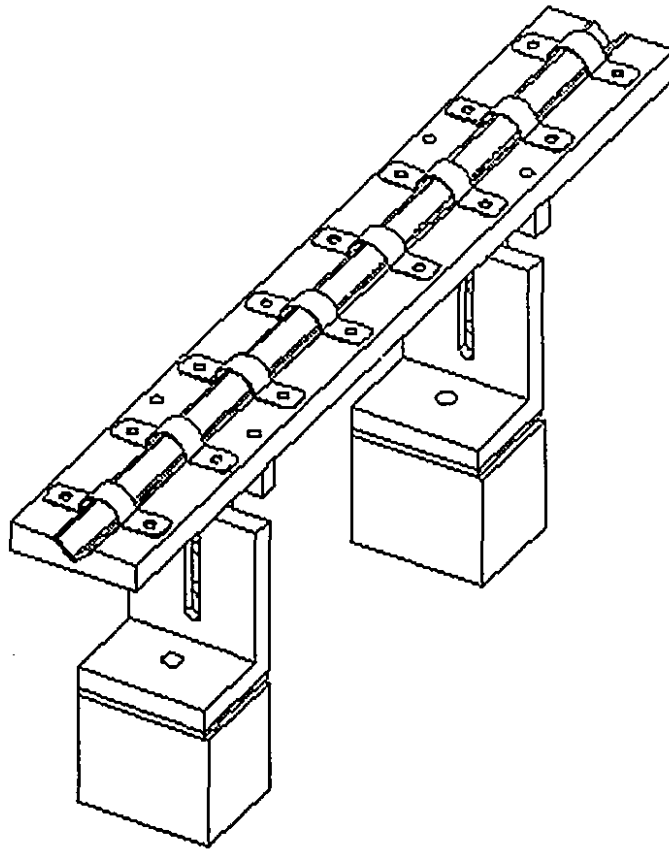


Figure 4.7 The slide

Protection rings are installed over the groove to prevent the bar from going off axis in case the gun is loaded improperly. Detectors for the velocity measurement of the striker are installed at the end of the slide. They consist of two infrared beams. The overall system will be introduced later.

The gas gun

A gas gun was chosen as the means of propulsion for the striker. It is the most common choice of device used with Hopkinson bar systems. It permits a wide range of speeds just by adjusting the pressure. The gas used is prepurified Nitrogen. It is an inexpensive and safe choice. The pressure is limited to 200 psi by the two stage pressure regulator. Figure 4.8 shows a cross section of the gas gun.

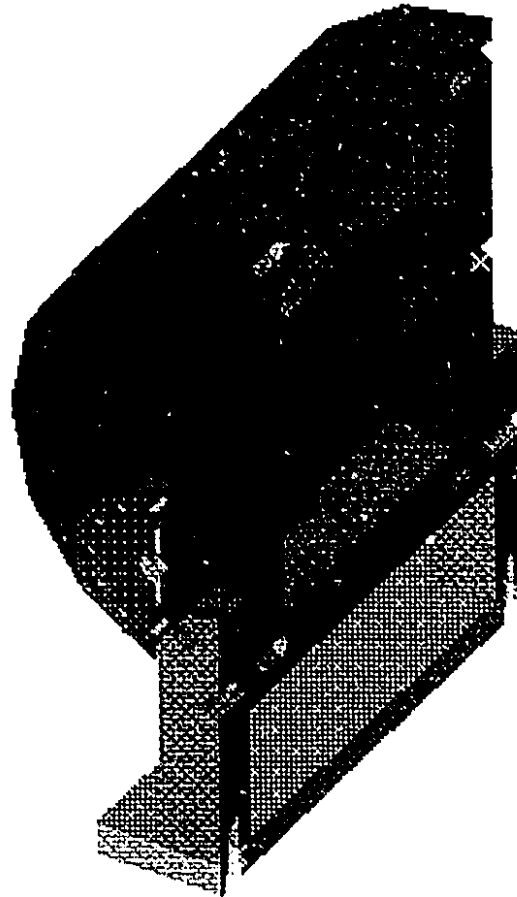


Figure 4.8 Gas gun section

The gun works in two steps. In the initial stage, the bar is loaded all the way to the back. In that position, the sabot blocks the vent holes going from the outer chamber to the inner chamber. The operator then opens the valve pressurizing the outer chamber. The inner chamber stays at the atmospheric pressure as there is no path for the gas to enter.

In the second step, the operator opens the second valve. This puts pressure directly behind the sabot pushing it ahead. This movement frees the vent hole and the pressure accumulated in the outer chamber reaches the back of the sabot. The sabot is then rapidly accelerated pushing the striker in front of it. At the end of the barrel, the sabot is stopped and the bar continues by itself. For the next shot, the striker will have to be loaded once again pushing the sabot to the back.

The speed of the bar is directly related to the pressure used. If friction and wave propagation are neglected, equating the work done by the pressure to the kinetic energy of

the bar and sabot will give the speed reached.

$$P A \Delta S = \frac{(M_s + M_b) V^2}{2} \quad (4.8)$$

Where

- P = Pressure
- A = Sabot cross section area
- ΔS = Barrel length
- M_s = Mass of the sabot
- M_b = Mass of the bar

The velocity can be expressed in terms of pressure by rearranging the equation. All the constant terms can be replaced by a constant K, which yields

$$V = K \sqrt{P} \quad (4.9)$$

This formula was used in the design process to determine the required pressure. This gives a general relation between the velocity and the pressure. Nevertheless, the neglected terms are not insignificant, and it is necessary to measure the velocity independently during the experiment.

The gun has been designed to be very safe. It can support the maximum pressure given by the regulator with a safety factor of 5. For the working pressure for this thesis, it has a safety factor of approximately 20. Most of the dimensions for the gun were chosen for practical reasons like machining and geometry purposes. Strength considerations were of concern only for the fasteners.

The gun is the only system component to be tightened to the table. Six 1/4 inch pressure bolts are used. This was done to prevent any kickback when firing the gun. The

magnets were not believed to be strong enough.

The momentum trap

The momentum trap consists only of a bar clamped in a big box. The box is free to slide and the momentum needed to displace it is enough to absorb the energy of the bar.

The Alignment

Every mechanical element of the system has to be well aligned to prevent moments and off axis loads. As the gun is the only permanently fixed unit everything will be aligned according to it. No special technology is used. The way to check if two components are well aligned is by visual inspection and by friction feeling. Even a small misalignment will result in friction, large enough to feel by moving and turning the bar. A level was also used to quickly obtain the horizontal alignment. Laser alignment techniques were investigated, but judged to be too expensive for the ease of alignment expected.

The first thing to align is the slide. A striker bar inside the gun will provide the reference for it. Then, the incident bar is aligned with the slide. In a third step, the transmitted bar is aligned with the incident one. The punch must be able to turn inside the die. There is 0.03 ± 0.02 mm of radial clearance. The last thing to do is to put the momentum trap in position. It requires only to have a clear contact with the bar. The slide and the momentum trap will have to be repositioned after each shot. The slide is most of the time removed to load the gun easily. The momentum trap is for its part, displaced while doing its function. It is recommended to check the bar alignment between every experiment but usually everything stays in place.

Electronic equipment

There are two main categories of electronic equipment in the Hopkinson Bar apparatus. The purpose of the first one is to read the magnitude of the strain pulses going

through the bars. The second one calculates the speed of the striker. Each is discussed below.

Strain pulses acquisition

Strain gages are used to measure strain in both the incident and the transmitted bars. It is desired to have a strong enough signal to be able to read it directly without the use of an amplifier. There are high frequency fluctuations in the signal which would require a special and expensive amplifiers. One way to avoid that problem is to use ceramic strain gages. This has been done by the two laboratories visited and was not recommended. Those gages are very hard to install and expensive; learning to install them may be costly. Finally their gain is not linear; the data manipulation is more complex to do. The second way is to use high resistance standard gages with a high voltage.

The second method was chosen. 1000 ohms resistors (Measurements group EA-06-250BK-10C) were used in a half Wheatstone bridge. Only 10V were put across it which was sufficient to read a full scale. Figure 4.9 shows the wheatstone bridge conditioning circuit used. The method to balance the circuit comes from Bazergui [16].

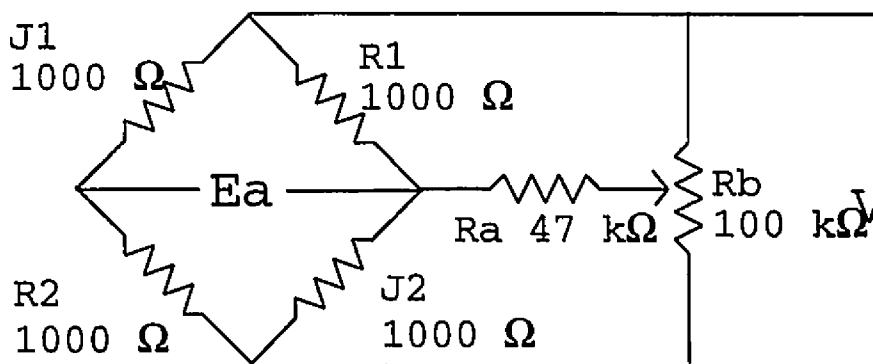


Figure 4.9 Wheatstone bridge

The oscilloscope used is a Nicolet Pro 40. It has 12 bits of vertical resolution and its maximum sampling rate is 10 MS/s. It is needed to record as many points as possible during the short duration of the experiment. The waveform treatment was done on the oscilloscope. It offers the possibility to program certain functions. The force vs time waveform and the displacement vs time waveform are calculated from the incident and transmitted pulses (see figure 4.10 to 4.13). The operation is performed on the digital

oscilloscope in which the equations presented earlier (4.5 and 4.6) are programmed. For the results presentation, the waveforms were taken to a Macintosh computer.

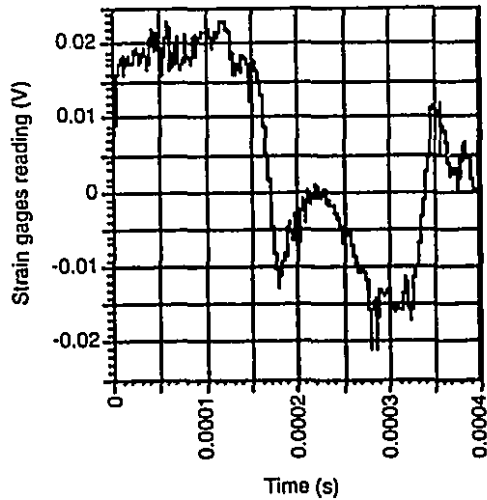


Figure 4.10 Incident bar reading

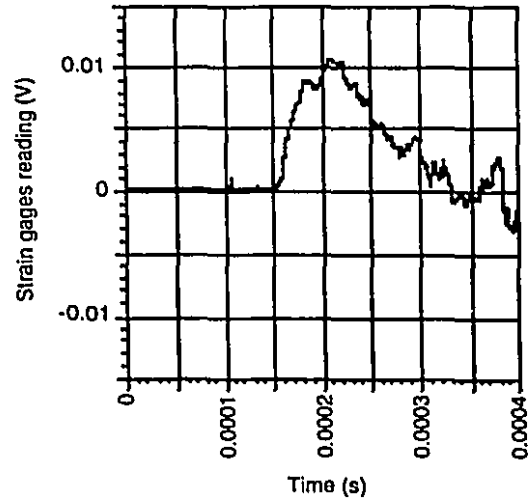


Figure 4.11 Transmitted bar reading

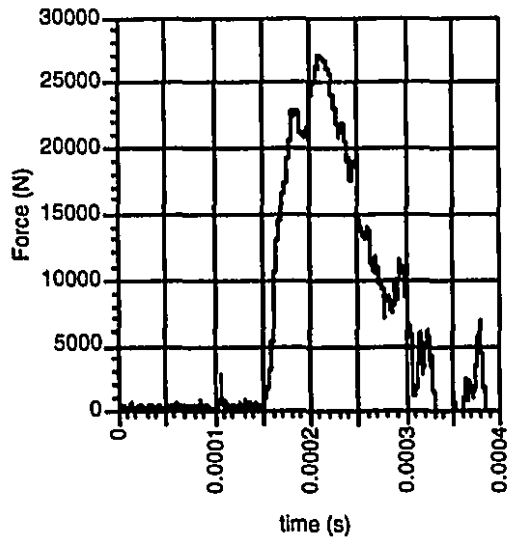


Figure 4.12 Force History

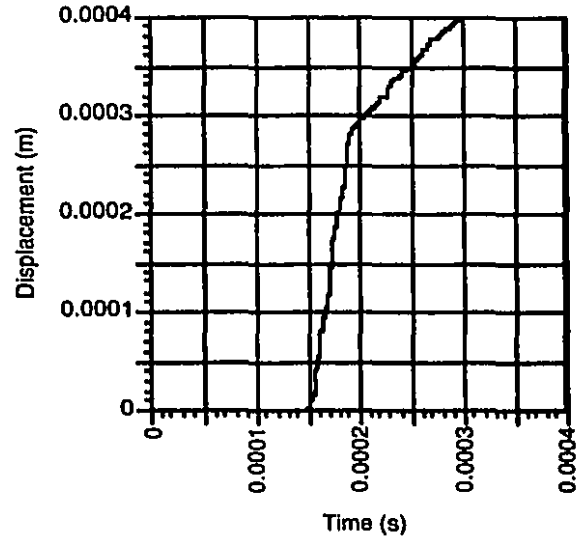


Figure 4.13 Displacement History

Calibration

The data acquisition system was calibrated by two different methods. First by putting a resistor in parallel with a strain gage (shunt resistor). Then the calibration was

checked by looking at the pulse from a striker of known velocity. The two results agreed.

The resistor put in parallel was chosen to produce a voltage variation similar to the one met during the tests. Its value is 219.7 k Ω and it produces a voltage variation of $\Delta E = 11.5$ mV. The relation joining ΔE to the strain ϵ is:

$$\Delta E = 10.6 \epsilon_i \quad \text{V} \quad (4.10)$$

Putting those values back into 4.5-4.7 and using the other known values, (4.5), (4.6) and (4.7) become:

$$\begin{aligned} \Delta U &= \int_0^t 360 \Delta E_i - 925 \Delta E_R \, dt \quad \text{m} \\ F &= 2.54 \times 10^6 \Delta E_t \quad \text{N} \\ V_i &= 923 \Delta E_i \quad \text{m/s} \end{aligned} \quad (4.11)$$

The last relation is used to check this calibration against the speed calculated on the slide.

Speed detector

The speed of the striker is calculated from the time that the bar takes to cross two infrared beams. These beams are located at the end of the slide and are 5.0 cm apart. At this location, the bar is completely out of the gun and travels at a constant speed. A NES Slimline DS1559 timer calculates the elapsed time between the two events.

The beams consist of photodiodes sending infrared light to lensed phototransistors. Light keeps the current going through the phototransistor. When the beam is cut, the logic circuit goes to 0. The timer itself is activated and stopped by a logic 0 at its different ports.

The problem encountered in this system is that the bar does not only pass through, it bounces back on the incident bar and crosses the beam again. As a result, the beam reading cannot control directly the timer. A more complex system has to deactivate the beams once crossed. The signal from the second beam will first go through a monostable multivibrators (SN74121) that will produce a square pulse. This triggers a relay. That

will, at the same time, stop the timer and deactivate the first beam. Schematics of the circuit are shown in appendix pp. 63-85.

Figure 4.14 shows the general Hopkinson system as it was built and used. The definition drawings for the parts that had to be built are appended to this report. (appendix p 63)



Figure 4.14 McGill University Hopkinson bar system A) bars B) Nitrogen tank
C) oscilloscope D) gas gun and slide

4.2-Static tests

The static tests were performed on an MTS 810 material testing system. A fixture was designed for punching tests by Thomas [13] . Figure 4.15 shows a representation of the fixture.



Figure 4.15 Static fixture

The MTS data acquisition system was not able to record data at the rates required for the medium rate tests. It was bypassed and the digital oscilloscope used for high rate testing (Nicolet Pro 40), was linked directly to the controller. Force vs time and displacement vs time data were collected and brought to a Macintosh computer for treatment.

The displacement measured was the stroke of the machine. It takes into account the fixture and the machine deformation. These effects have to be measured to subtract them from the specimen displacement. A rod of the same area and material than the die was inserted into it. A compression test on the fixture is then performed. Figure 4.16 shows the force displacement graph for the fixture.

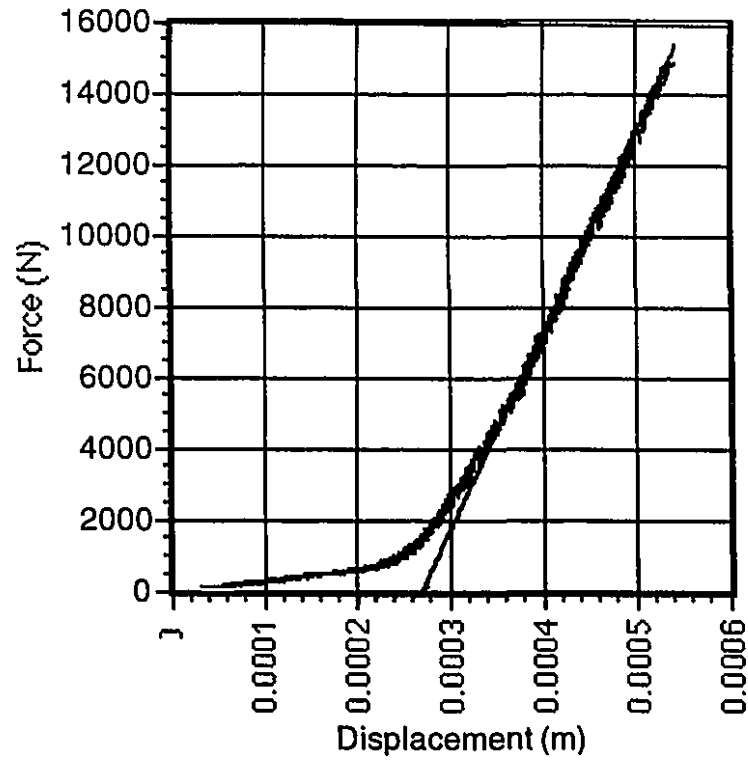


Figure 4.16 Fixture response (curve) and model (linear)

The behavior is mostly linear; only the first part of the curve is not. The fixture displacement will be modeled only with a linear formulation. The formula used to correct the displacement is:

$$\Delta u' = \Delta u - \left(\text{force} / 5.6 \times 10^7 + 2.7 \times 10^{-4} \right) \text{ m} \quad (4.12)$$

The correction neglects the first part of the curve.

5-Material

A standard material AS4/3501-6 (graphite/epoxy) was chosen for the test, using a quasi-isotropic laminate. In this way, the punching experiment can be considered to be axisymmetric, which reduces the analysis considerably. Other punching experiments [9] have shown that less scatter was observed with thicker specimens. Therefore, a 24-ply (3.3 mm) laminate has been chosen. The actual lay up is [+45/-45/0/90]_{3s}.

Two 0.3m square (12in X 12 in) plates were made at the Centre Des Matériaux Composites de Saint-Jérôme. The pressure and temperature curing cycles are presented in appendix p.86. The quality of the plate was checked by ultrasonic c-scan. The result is presented in appendix p.87. It indicates no significant defect. Only plate number 88388111 has been used for this study.

The plate was cut in 3.8 cm square specimens. It was done using a tile saw with a diamond blade. Water is used to cool down the material during the operation. The material is not damaged by this procedure. The size of the specimens was chosen to be large enough to minimize edge effects.

6- Test Procedures

Two categories of tests were performed:

- Tests on the MTS Machine;
- Tests on the Hopkinson bar.

On the MTS machine tests were performed at 3 different speeds. They are controlled by the tests duration. The total displacement chosen (specimen+fixture+machine) is specified for a specific time.

The tests use the designation:

- very slow: 10s;
- slow: 1s;
- medium 0.1s:

The temporal distribution of the displacement is set to be sinusoidal due to limitations of the equipment.

The medium rate is the maximum velocity that can be achieved. It is limited by the amount of oil the MTS machine can drop in a certain time.

On the Hopkinson bar apparatus the tests are controlled in a different way. The speed and the length of the striker control the parameters of the tests. The long striker bar was used for most experiments. It offers a larger range of speed where total penetration is possible. For any striker length, the maximum speed at which it can hit the bar is directly related to the yield stress of the bar material. Therefore, the maximum displacement rate for any striker is the same. The lowest displacement rate depends on the length of the striker. The longer the striker, the more energy it carries, the lowest speed it needs for perforation.

Perforation while still keeping the bars elastic is possible for the long striker at impact velocities from 13 to 19 m/s. Tests at slower speeds were also performed to investigate the behavior during partial penetration.

With both kinds of settings, interrupted tests were also performed. They are done to investigate the way the damage evolves in the material. The specimens are then X-rayed and cut for characterization.

7-Results

In this section, the results will be presented. Each kind of test presented will be discussed individually and then compared to each other. For each kind of test, from two to four different results will be plotted on the same graph to show the repeatability in the results.

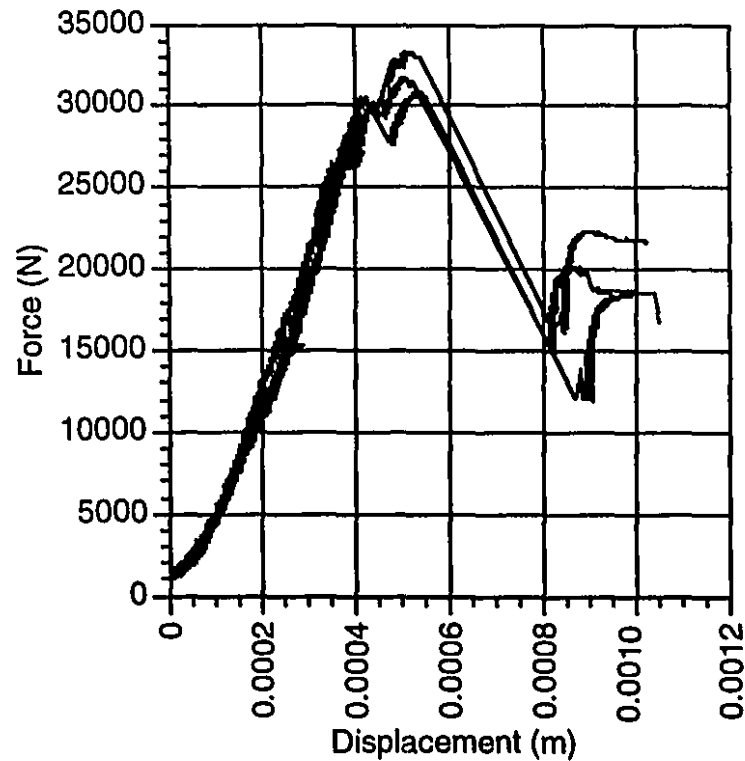


Figure 7.1 Punching speed = 0.001 m/s

Figures 7.1 and 7.2 show the results for a 10 sec duration test and a 1 sec one, respectively. This corresponds to 0.001 m/s and 0.01 m/s punching speed, respectively. In both cases, the curve can be separated into three parts. The first corresponds to the loading of the specimen. In that part the results are very repetitive. This zone goes to approximately a 0.4 mm displacement. This corresponds to a load of approximately 30 kN. The second zone corresponds to the actual punching of the composite. The results are less repetitive there. Even if the values obtained have some scatter, the general modes of failure stay the same. The shapes of the peaks are the same. The third zone corresponds to the plug being pushed out. The force needed to push the plug varies from specimen to specimen. Nevertheless, it stays in a relatively small range. Small variations in the way the specimen was damaged may cause bigger variations in forces.

The straight lines between what was called zone 2 and zone 3, from approximately .45 mm to .80 mm, correspond to lines of two points. There are no data points between the two ends of the line. This is caused by the fact that when the material breaks, there is a sudden drop in load. The MTS cannot react instantaneously and there is a jump in the displacement while it adjusts. A much higher sampling rate would be needed to get points in that region. The duration of the whole test does not permit such a sample rate. The amount of data obtained would be impracticable. This fact is shown by looking at figure 7.3. In that test, the punching speed was much higher, so the sampling rate is much faster. It was then possible to pick up the last part of that jump when the machine starts to stabilize.

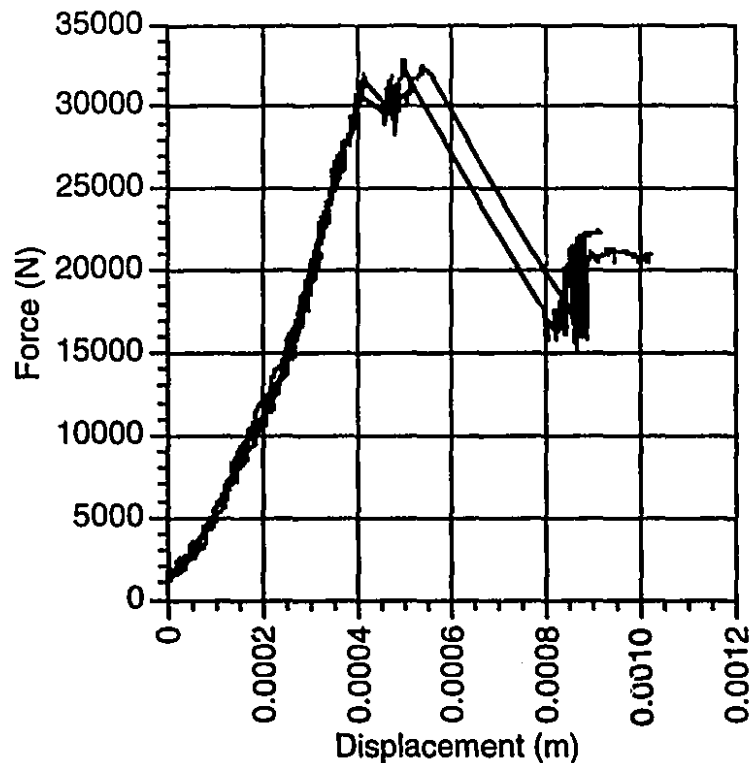


Figure 7.2 Punching speed = 0.01m/s

At a punching speed of 0.1 m/s, there is much more scatter. One of the tests performed even has a different slope. As this specimen also had an early failure, it was thought to be caused by a defect in the specimen. It is also important to mention that this test was performed at the maximum speed the machine can reach. There was considerable vibration in the system after the experiment. Due to the small duration of the test, it is

impossible to comment on the behavior of the machine during the test.

Figures 7.4 and 7.5 show the results for high speed punching when penetration was achieved. Figure 7.4 corresponds to the minimum striker speed (approximately 13 m/s) while figure 7.5 corresponds to the highest one (approximately 18 m/s). The average punching speeds related to those striker velocities are approximately 4.2 and 6.0 m/s, respectively. The average punching speed is calculated by dividing the total displacement by the experiment duration.

At high rates, the curves are more complex than at low ones. The first part of the loading corresponds to a straight line. All tests are very repeatable in this region. Then there is a change in the slope (softening). The point at which this happens varies slightly from specimen to specimen. A plateau is reached at approximately 22 kN. Following this, there is a rapid increase in force (stiffening) to get to the maximum load. In contrast to the slower tests, the maximum peak is reached first and then there are several lower peaks. Finally, the last part of the curve, if reached, is the plug being pushed out.

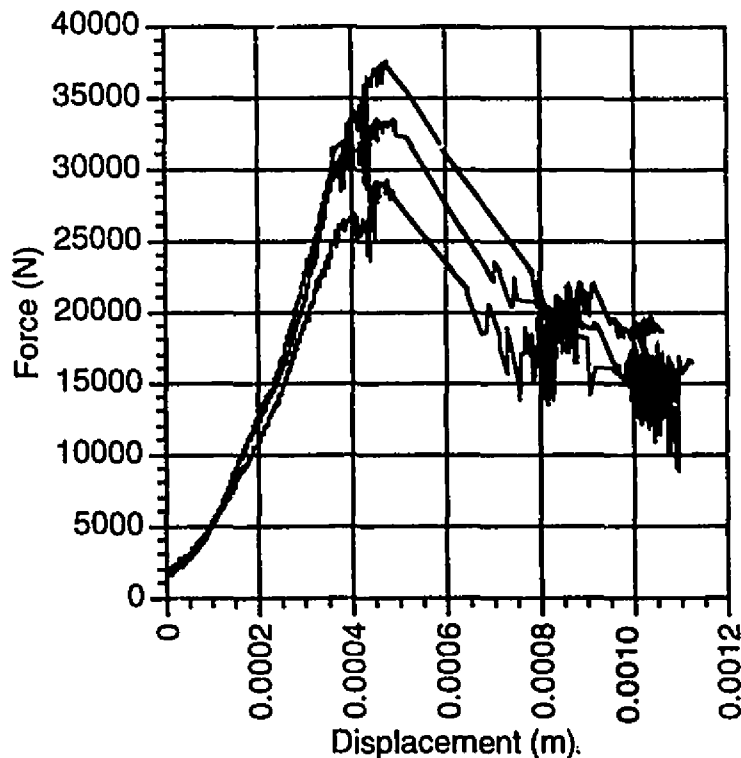


Figure 7.3 Punching speed =0.1 m/s

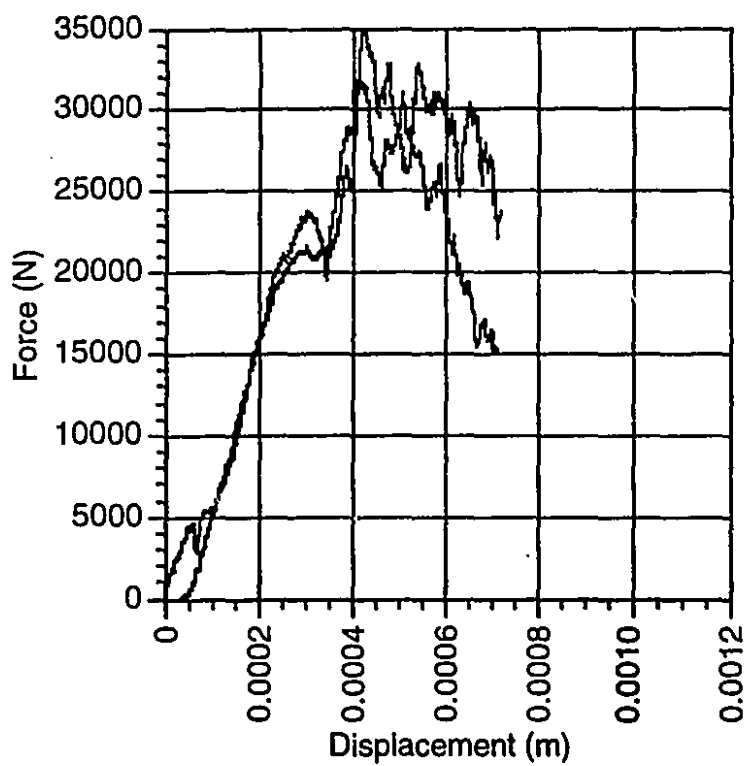


Figure 7.4 Punching speed = 4.2 m/s

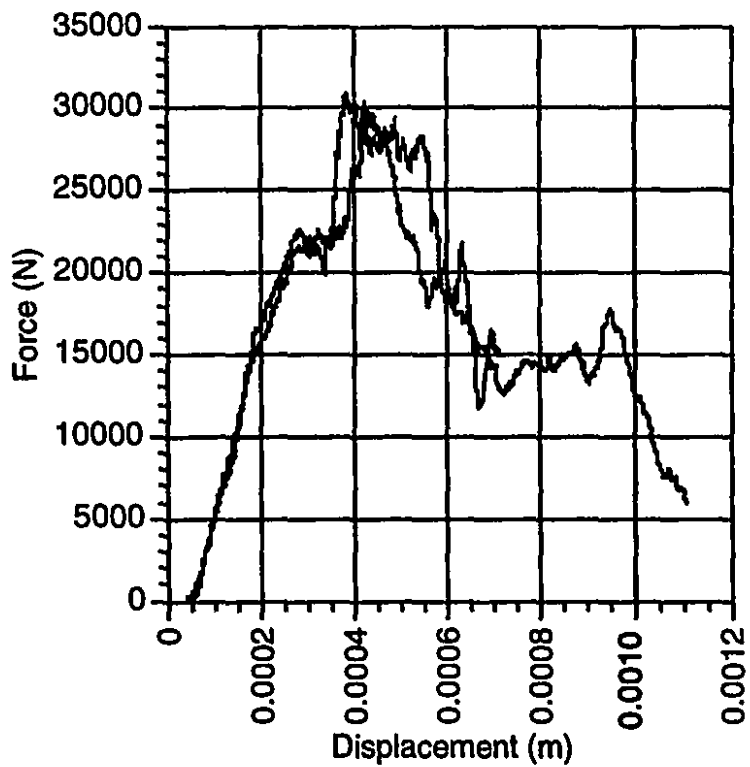


Figure 7.5 Punching speed = 6 m/s

Figure 7.6 compares the force/displacement results for tests conducted at speeds insufficient to completely punch through the specimen. The general appearance of the curves is the same as completed tests but the changes in slopes and the plateau seem to happen at lower values. There is little visible damage on those specimens when inspected. There is a small mark done by the punch on the surface. No significant damage is revealed by x-rays. Cutting the specimen and inspecting it show, however, if the load reached is high enough, some permanent deformation in the layers.

Figure 7.7 shows the influence of the punch finish on the results. The tests were performed with the punch not completely flat nor perfectly perpendicular. It resulted in some scatter for the first part of the curve. When the punch is not sufficiently perpendicular to the specimen, it will not hit it everywhere simultaneously. The curve, obtained when the bar is perpendicular lies in the middle of these other curves. The global behavior for the rest of the curve is still similar but a lot more scatter is observed.

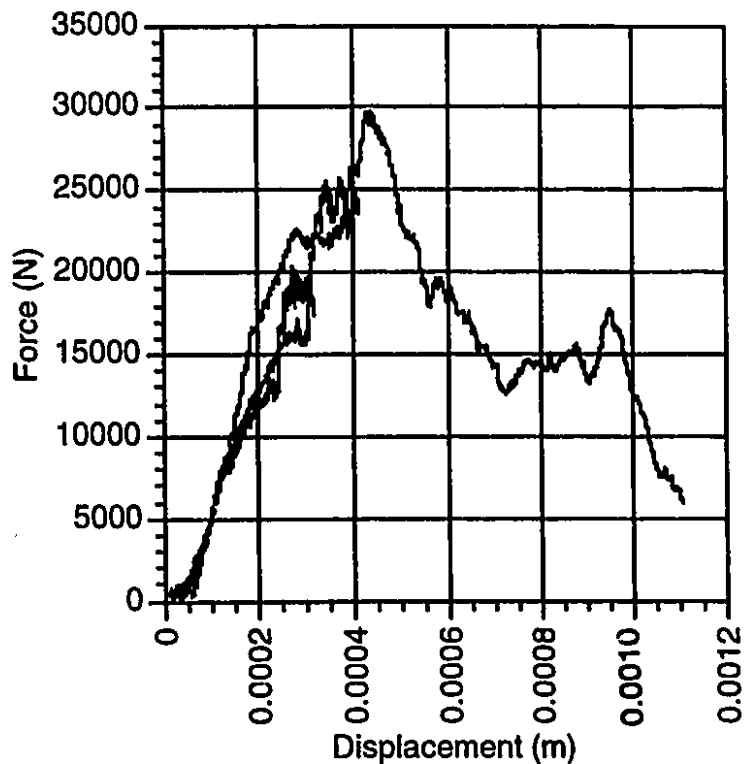


Figure 7.6 Comparison of lower striker velocity tests (8 and 10 m/s) to a 18 m/s test

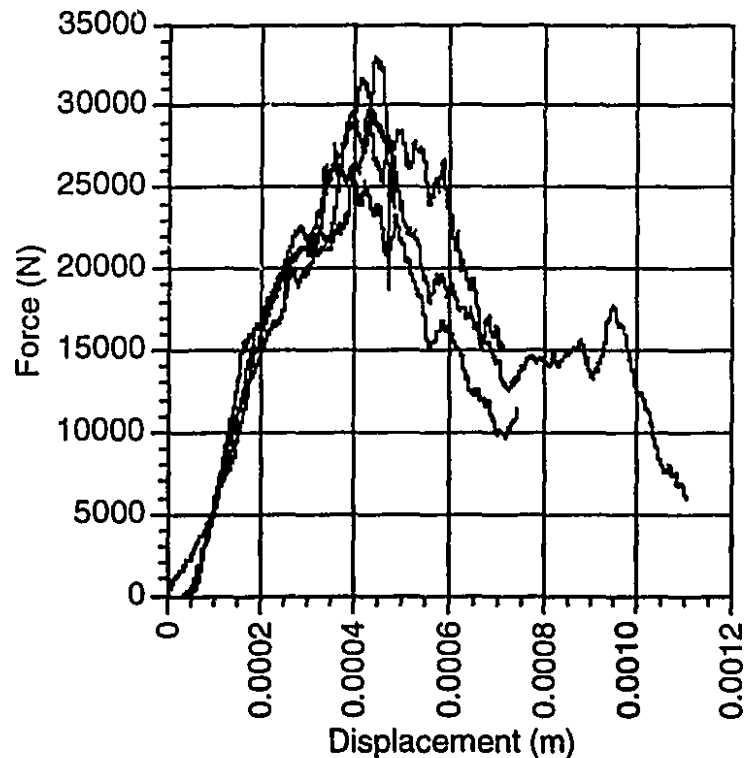


Figure 7.7 Effect of having the punch faces not perpendicular with the bar axis

7.1-Results comparison

Figure 7.8 investigates the difference between the two slowest tests. As the two curves are very similar, the differences are hard to detect. From the data it was found that the slope of the faster one is slightly larger. There is also a difference in the top part of the curve. It is easier to see by comparing figure 7.1 and figure 7.2. At the slower speed, the difference between magnitude of the two peaks is bigger. As those two types of curves are similar, only one will be referred to in the remainder of this discussion.

For the fast tests on the Hopkinson bars, there is little difference between the two rates. Figure 7.9 shows the superimposed results of figure 7.4 and 7.5. The first part of the curves are identical. Even the smaller velocity tests of figure 7.6 behave in the same way in that region. There is some difference where the curves soften. As the scatter in the results for that region is also higher no definite conclusion can be reached on this difference.

In general, the difference in displacement rates for these two punching speeds is small (30%). This is not enough to show conclusive differences. These two tests will be referred to from now on as high speed tests and not differentiated.

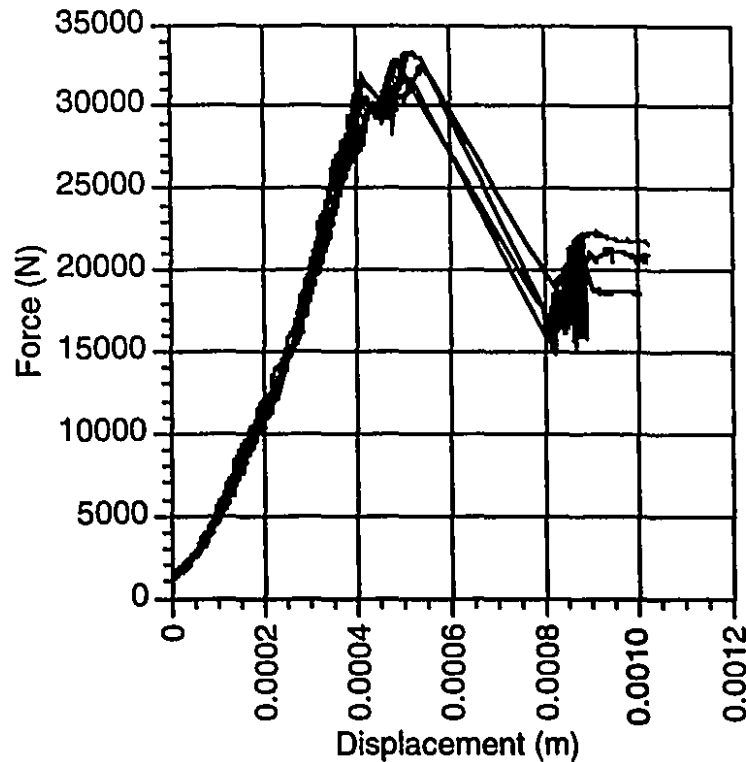


Figure 7.8 1 and 10 sec tests

The three selected curves: slow, medium and high punching speeds, are plotted together in figure 7.10. One of the important things to notice is the first part of the curves. A rise in punching speeds produces higher slopes. This is consistent with rate dependent behavior of most materials. It can also be related to tests on GFRP performed by Harding [9] who obtained similar behavior for the loading of the material. The other thing to notice is the peak value reached. As mentioned before, there is some scatter for the value even for the tests at the same punching speed. The difference found between different categories of tests lies within the scatter. With the large quantity of tests performed, the value seems to be constant for all strain rates.

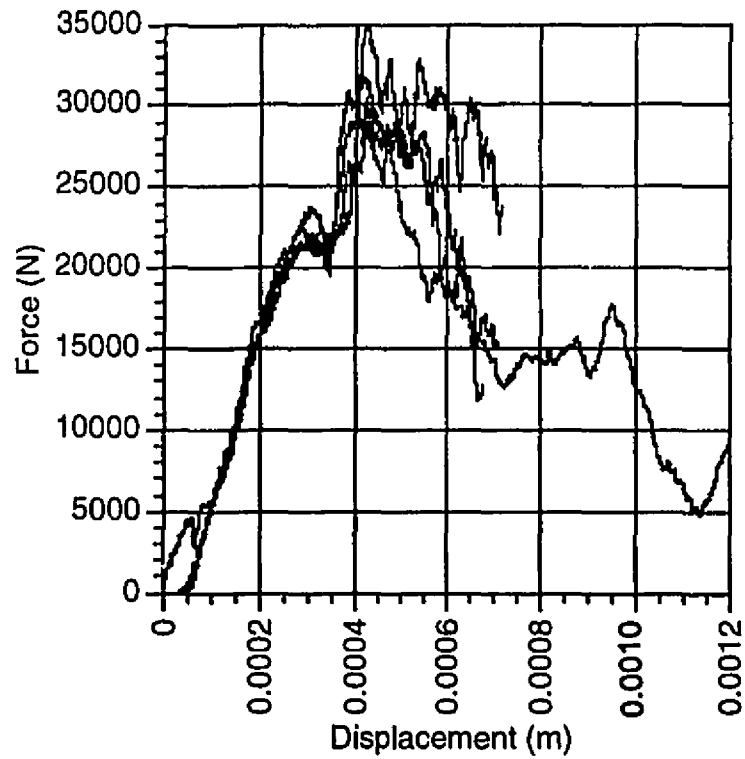


Figure 7.9 High speed punching

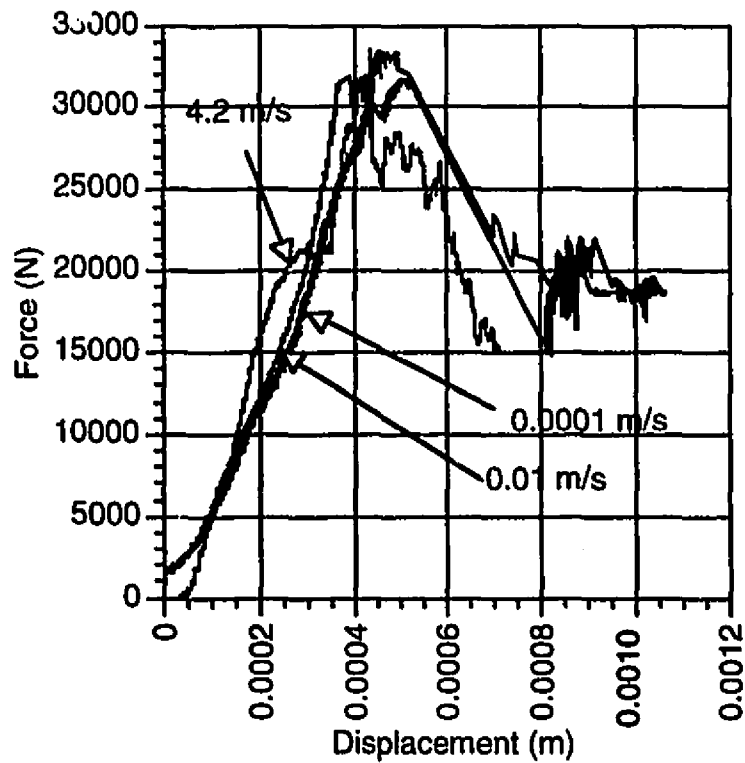


Figure 7.10 Three different modes

8-Specimen inspection

8.1-X-ray

Several of the specimens were x-rayed to investigate the extent of the damage. A dye was used to make the damaged regions show on the pictures. The dye is 1,4-Diiodobutane made by Aldrich Chem. Co. It was not put directly on the damaged region. The concentration of dye would have been too high to correctly analyze the pictures. The dye was applied on the edges of the specimens. It was then left to bleed in. Three to four applications were taken at one hour intervals. The dye permeates through the undamaged regions and accumulate in the damaged ones. The x-rays were done in a Hewlett Packard cabinet x-ray system, Faxitron series. The exposure was set to 10 sec and the tube voltage to 20 V. Figures 8.1 to 8.3 show the evolution of damage while punching.



Figure 8.1 Low punching load

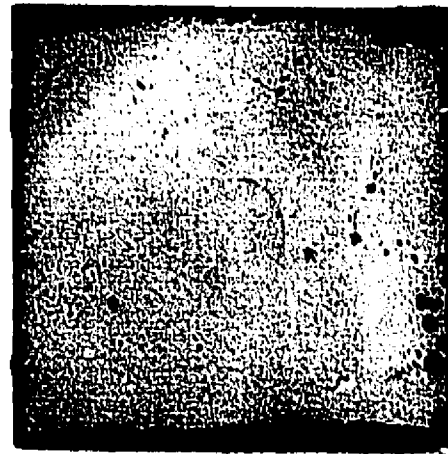


Figure 8.2 Almost punched

Figure 8.1 shows an interrupted test taken to 15 kN and no damage can be seen. Figure 8.2 shows a specimen that was submitted to a 25 kN punching load (approximately 80% of the maximum load). A crack begins to show around the punch. Figure 8.3 shows a completely punched specimen. The punched ring is clear, indicating that damage is concentrated in the narrow zone around the punch.

There is no apparent difference in damage between specimens punched at the various rates. There is no apparent edge effect indicating that the choice of specimen size is appropriate. The first three figures do not show the damage in the plug. The dye that comes from the edges of the specimen stops in the crack around the plug. It does not reach its inside region. Some dye was directly applied in the lightly damaged region of the specimen shown in figure 8.4. The damage in the plug is then shown. This method could be used for this specimen because almost no cracks were present on the surface of the specimen. Only a small amount of dye then penetrates. The specimen shown in figure 8.4 was at the onset of complete failure; the maximum load was a little bit over 30 kN. A section of the same specimen will be shown in the next section.

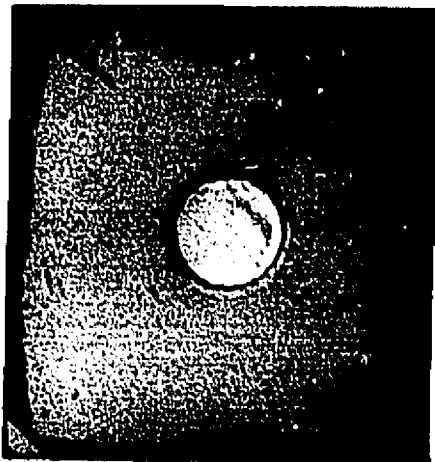


Figure 8.3 Punched specimen

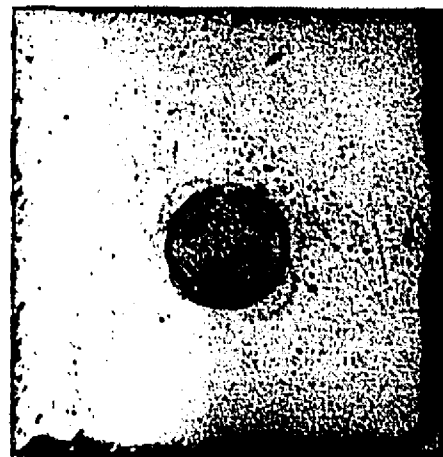


Figure 8.4 Dye applied on the plug



Figure 8.5 Holders effects

Specimen holder effects were also investigated. The x-rays shown from figure 8.1 to 8.4 come from tests where the specimen is held only by the pressure bars and the support screws. The holder is only used for protection and has no effect on the specimens. Contact between the specimens and the support during an experiment would change test conditions. A portion of the transmitted wave would go through the support, and the Hopkinson bars principles would not apply anymore. Figure 8.5 shows the damage region for a test in which this event occurred. The support geometry is imprinted in the damage region.

8.2-Visual inspection

To observe the damage inflicted to the laminates at different stages of punching, the specimens were cut in two. The same tile saw used for cutting the specimens to size was used for sectioning. As the specimens were not always punched exactly in the center, it was difficult to exactly split the punching region in two. Furthermore, the saw cutting line is fairly thick (1.5 mm) resulting in a loss of material. These two facts explain why on the presented pictures, the punched region is neither exactly the same nor directly related to the die diameter.

The images were acquired using a black and white digital camera linked to a microscope. Visual inspection is made easier by the presence of white lines. These lines are produced by the 0 or the 90 degrees plies depending on which orientation the specimen was cut. The white color is produced by the light reflecting on the fibers parallel to the cutting line. One thin white line represents one ply. The thick dark gray lines represent two or three plies depending on its width.

Figures 8.6 to 8.10 show the different stages of punching. Once again, no macroscopic damage differences were observed between slow and high rate punching. In all figures, the punched side is at the bottom. Figure 8.6 shows a cut specimen to which was applied a 21 kN punching load. The material does not show much damage but some permanent deformation is present. A horizontal line has been drawn along one ply to make this easier to visualize. Some rotation of the fibers is present in the sheared region.

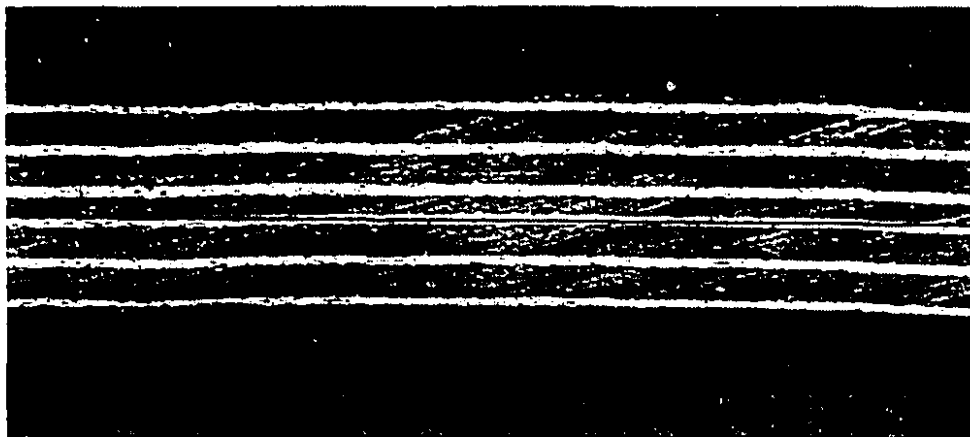


Figure 8.6 21kN load

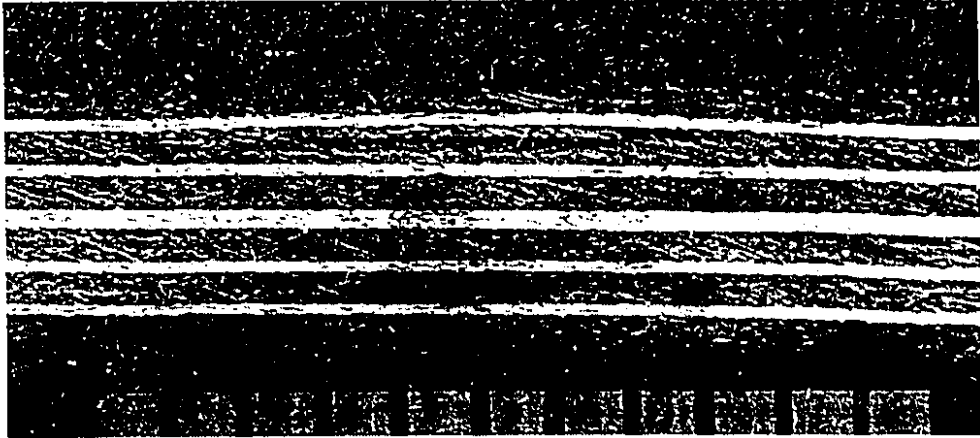


Figure 8.7 31kN load

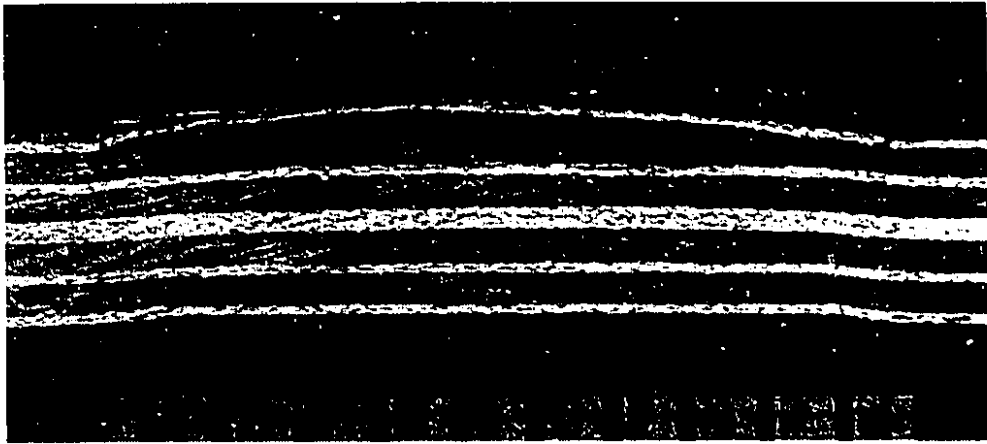


Figure 8.8 Maximum load reached

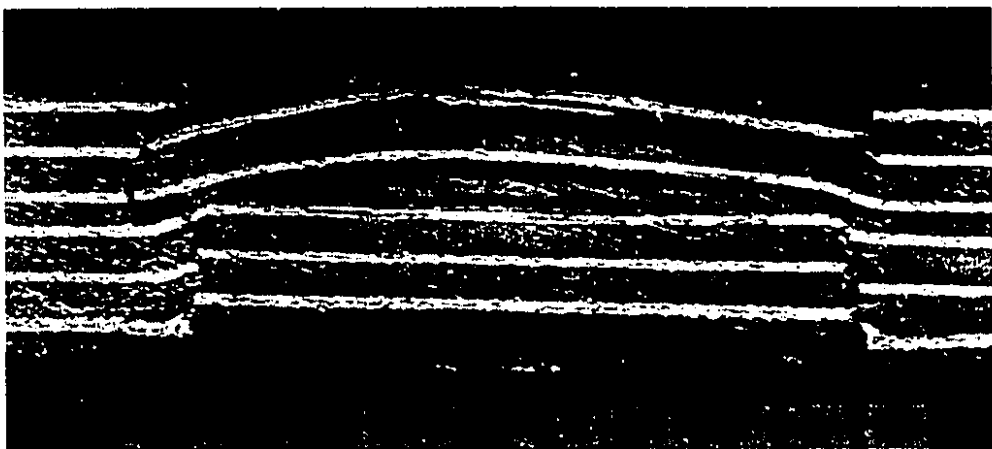


Figure 8.9 Completely punched specimen

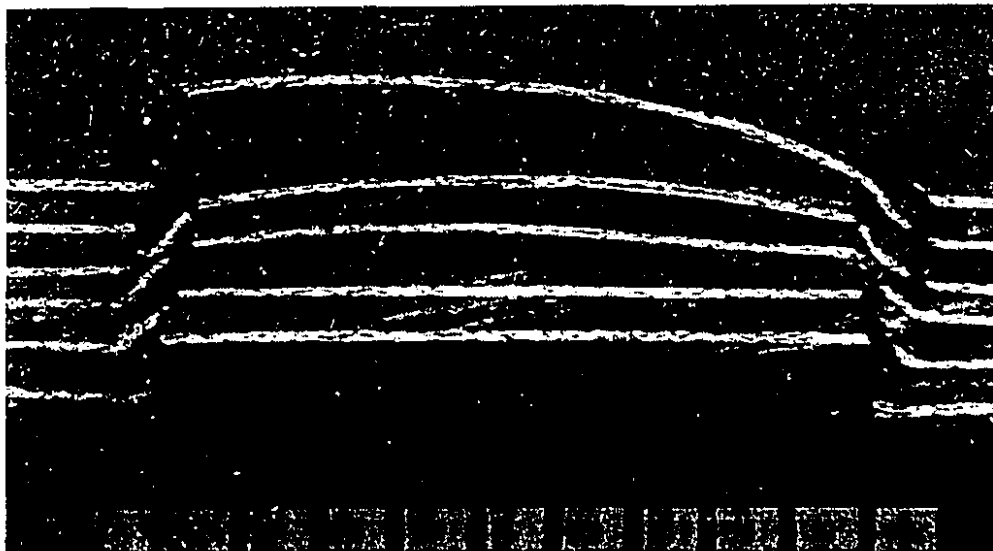


Figure 8.10 Plug being pushed out

Figure 8.7 shows a specimen subjected to a 31 kN punching load. The x-ray of that same specimen was presented in figure 8.4. The peak load was almost reached and some damage is apparent. A lot of interlaminar delamination is present in the lower plies.

The specimen of figure 8.8 was damaged a little further. The peak load was reached and the sample had already lost much of its strength. The delamination in the lower plies is more pronounced. Transverse cracks are appearing where the plies are rotating.

In figure 8.9, the specimen has lost mostly all its strength. The load at this stage is only that needed to push the plug out of the specimen. Delamination is present in the lower half of the specimen. The transverse cracks are more apparent than in the previous picture. Two different cracks are present: one on the top half and one on the bottom half of the specimen. The top one is going inward as it is going down while the bottom one is going outward as it is going up. A horizontal crack links the two.

Figure 8.10 shows the plug being pushed out of the specimen. The region between the two cracks completely rotates. The plies form a bubble on the lower surface before being completely separated. The delamination zone is extended even further toward the top of the plug.

9-Modes of failure

The information gathered by the specimen inspection of the last section will help formulate the damage evolution.

During the loading of the specimen, which corresponds to the first part of the load-displacement curve, the principal mode of damage is believed to be matrix cracking. Figure 8.6, which shows only a small permanent deformation, correlates with this idea. The rate-dependence observed in that part of the curve would be related to the time dependent material response through the damage process, which in that case is matrix cracking.

When the punch further deforms the material, the rotation in the sheared region reaches a level where the fibers come into tension. It is as if the punch was supported by a net and to go through, it has to break the threads. Even if the matrix is considerably damaged, the fiber can support the load. The maximum load that can sustain the material is then dictated by the tensile properties of the fibers. This explains why the maximum load does not vary with the strain rate, since the tension properties of graphite fibers have previously been shown [5] not to vary with strain rate.

The maximum peak is not always the first one (see figure 7.1). At some strain-rate, a lower peak is first reached. It is postulated that at this peak some fibers fail, letting the entire system move with a lower force for a while until a stronger configuration is reached. Even if the maximum force is reached on the first peak, subsequent ones usually follow. A lot of damage occurs while going from one peak to another.

While reaching the peak load, the matrix is considerably damaged. Where it has to rotate to permit the fibers to take the load, the matrix is sheared. There is also delamination present mostly in the lower part of the specimen. As the sample is relatively thick, differences in the modes of failure of the top and bottom parts occur.

When the load drops considerably, the material is completely cracked. The cracks are not going straight from the top to the bottom. To push out the plug, some load is needed to deform the material on the edges of the cracks. Localized rotation occurs permitting the plug to go through the smaller regions.

10-Recommended further research

There are many facets related to this experiment that would be interesting to investigate.

First it would be interesting to study the influence of the lay-up on the punching properties. The lay-up effects on a drop test with a steel ball have been studied by a few authors [17-18]. Different results have been obtained. The use of a more simple experiment, such as the one performed here, could bring new insights to the problem. In this experiment, a quasi-isotropic configuration has been used to retain axisymmetric loading. Studies of other lay-ups need to be performed.

In addition, the influence of the constituent would give some interesting information. In this work, the maximum load was found to depend on the tensile properties of the carbon fibers. As this property does not vary with rate, the load is constant. By using glass fibers, which are rate dependent, a different behavior would be obtained. Harding [9] obtained much different results when he did tests with GFRP. In the same way, using a different matrix would probably influence the first part of the curves.

Finally, it would be interesting to study the effect of the sample thickness. The damage observed in this experiment was not constant throughout the thickness. A thinner specimen would exhibit different modes of failure.

11-Conclusion

A punching test was designed to characterize the transverse shear properties of laminated graphite/epoxy composites for different strain rates. The tests were performed on a MTS machine at slow and medium speeds and on a Split Hopkinson bar apparatus for higher velocities. The tests were successful and good repeatability was obtained.

The loading part of a force/displacement curve is believed to reflect the matrix cracking response of the material. It is found to be rate dependent. The peak value is believed to be linked to the tensile properties of the fibers, which for graphite fibers are rate-independent. After significant rotation, the fibers are loaded in tension. It explains why the peak load does not vary with strain rates.

The modes of damage are found to be more complex than what could be expected in such an experiment. Matrix cracking is the first damage encountered followed by delamination and finally by fiber failure. The damage is localized in the punched region.

A finite element analysis of the system, using a damage model and the results from those experiments, will bring more insight to the damage progress. The effects of the lay-up, the specimen thickness and the constituent would be interesting to investigate.

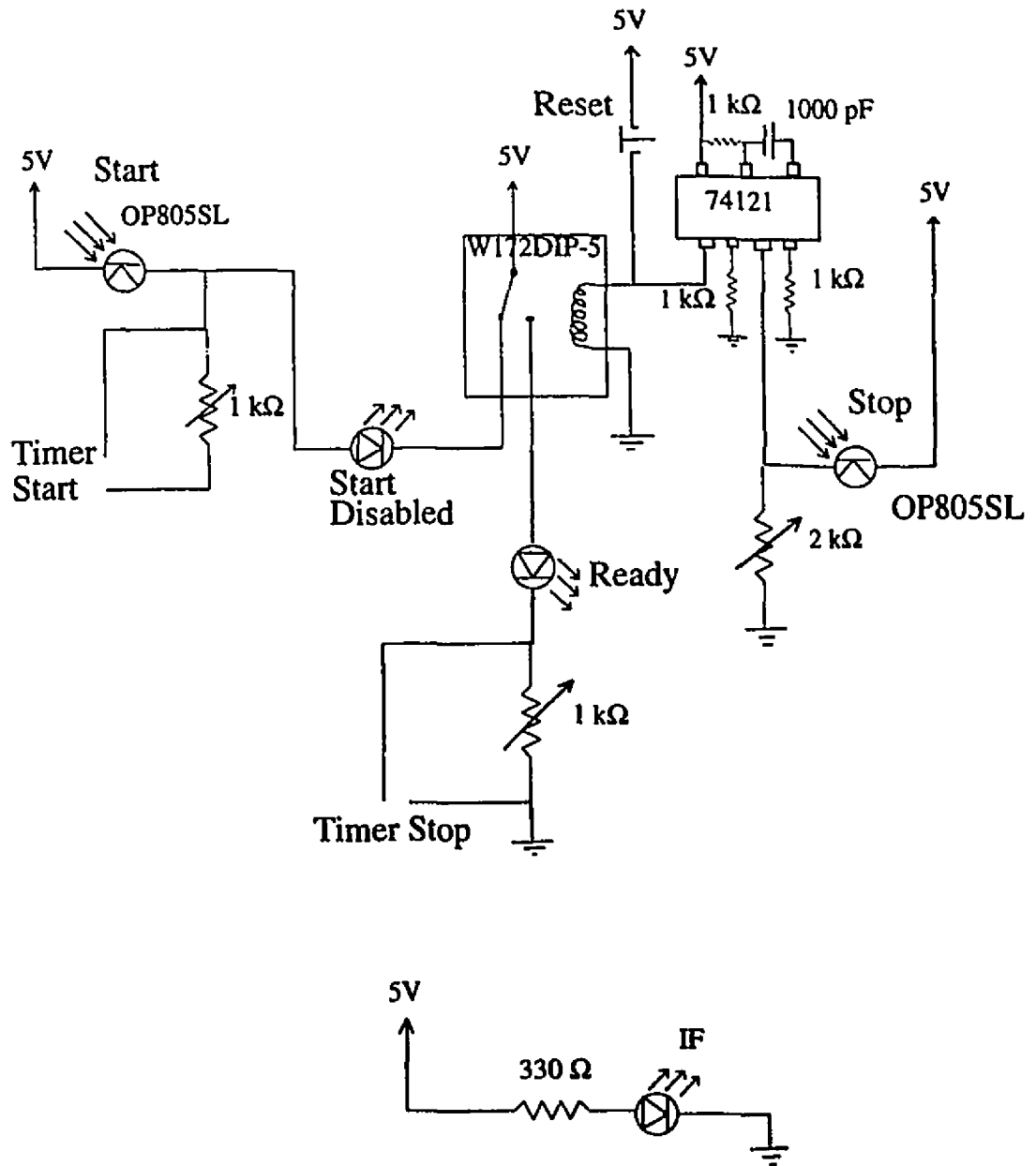
Overall, the rate dependence found in this experiment is considered to be significant for loading conditions such as impact.

REFERENCES

1. Macaulay, M.A. Introduction to impact engineering, 1987, Chapman and Hall.
2. Newill, J.A. and Vinson, J.R. "Some high strain rate effects on composite material", Proceeding of the ninth international conference on composites materials (ICCM/9), Madrid (1993), Volume V, 269-277.
3. El-Habak, A.M.A., "Mechanical behavior of woven glass fibre-reinforced composites under impact compression load", Composites, Vol 22, No 2 (1991), 129-134.
4. Staab, H.G. and Gilat, A., "High strain rate characterization of angle-ply Glass/Epoxy laminates", Proceeding of the ninth international conference on composites materials (ICCM/9), Madrid (1993), Volume V, 278-285.
5. Harding, J. and Welsh, L.M., "A tensile testing technique for fibre-reinforced composites at impact rates of strain", Journal of materials science 18 (1983), 1810-1826.
6. Werner, S.M. and Dharan, C.K.H., "The dynamic response of graphite fiber-epoxy laminates at high shear strain rates", Journal of composite materials, Vol. 20 (1986), 365-374.
7. Bouette, B. and Cazeneuve, C., "Effect of strain rate on interlaminar shear properties of carbon/epoxy composites", Composites Science and technology 45 (1992), 313-321.
8. Lataillade, J.L., Delaet, M. and Collombet, F., "Damage testing of crossply laminates under high strain rates. Effects of intralaminar shear stresses", Journal of materials science letters, (1992), 358-365.
9. Harding, J., "The high-speed punching of woven-roving glass-reinforced composites", Inst. Phys. Conf. Ser. No. 47: Chapter 3 (1979), 318-330.
10. Sun, C.T. and Grady, J.E., "Dynamic delamination fracture toughness of a graphite/epoxy laminate under impact", Composites science and technology 31 (1988), 55-72.

11. Lee, S.-W. R. and Sun, C.T., "Dynamic penetration of graphite/epoxy laminates impacted by a blunt-ended projectile", *Composites science and technology* 49 (1993), 369-380.
12. Randles, P.W. and Nemes, J.A., "A continuum damage model for thick composite materials subjected to high-rate dynamic loading", *Mechanics of materials* 13 (1992), 1-13.
13. Thomas, N., "Analysis of the punch shear experiment for Graphite/Epoxy composites", Unpublished.
14. Staab, G.H. and Gilat, A., "A direct-tension split Hopkinson bar for high strain-rate testing", *Experimental mechanics*, Vol.31, No.3 (1991), 232-235.
15. Follansbee, P., "The Hopkinson Bar", *Metal Handbook*, Ninth edition, Volume 8 (mechanical testing), 198-203.
16. Bazergui, A., "On the initial balance of Wheatstone bridges", *Strain*, Volume 7, No 1.
17. Strait, L.H., Karased, M.L. and Amateau, M.F., "Effects of stacking sequence on the impact resistance of carbon fiber reinforced thermoplastic toughened epoxy laminates", *Journal of composite materials*, Vol. 26, No. 12 (1992), 1725-1741.
18. Choi, H.Y., Wang, H.S. and Chang, F.-k., "Effect of laminate configuration and impactor's mass on the initial impact damage of graphite/epoxy composite plates due to line-loading impact", *Journal of composite materials*, Vol. 26, No. 6 (1992), 804-827.
19. Zukas, J.A. et al. Eds., *Impact dynamics*, John Wiley and Sons, New York, 1982.
20. Dowling A.R., Harding, J. and Campbell, J.D., "The dynamic punching of metals", *Journal of the institute of metals*, Vol. 96, (1970), 215-224.
21. Hibbitt, Karlsson & Sorensen, inc, *ABAQUS user manual* Pantucket RI, 1994
22. Timoshenko, s., *Theory of plates and shells*, McGraw-Hill Book company, 1940, pp. 55-84

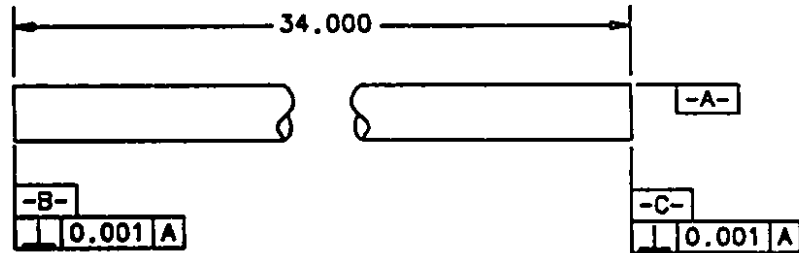
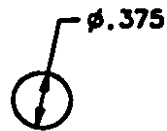
Appendix



Timer control circuit

Notes:

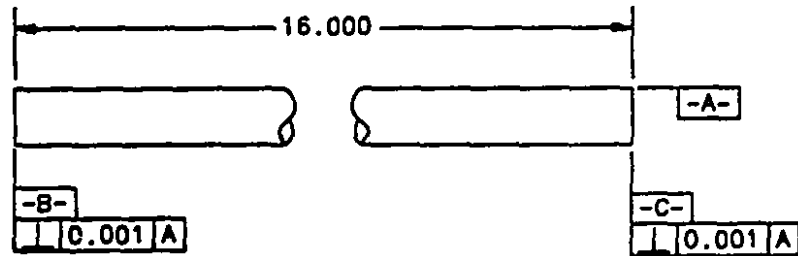
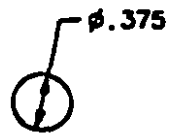
- 1-Material: Tool steel O1
- 2-Bar already ground
- 3-Remove one inch from each end
- 4-Surface roughness to be 53 microinches on both ends



Hopkinson Bars System		McGill University	
Drawing Incident bar		By Sylvain Riendeau 398-5037	
Scale	Date 4-01-94	General Tolerance ± 0.005	No HBS-01-01 Version 1

Notes:

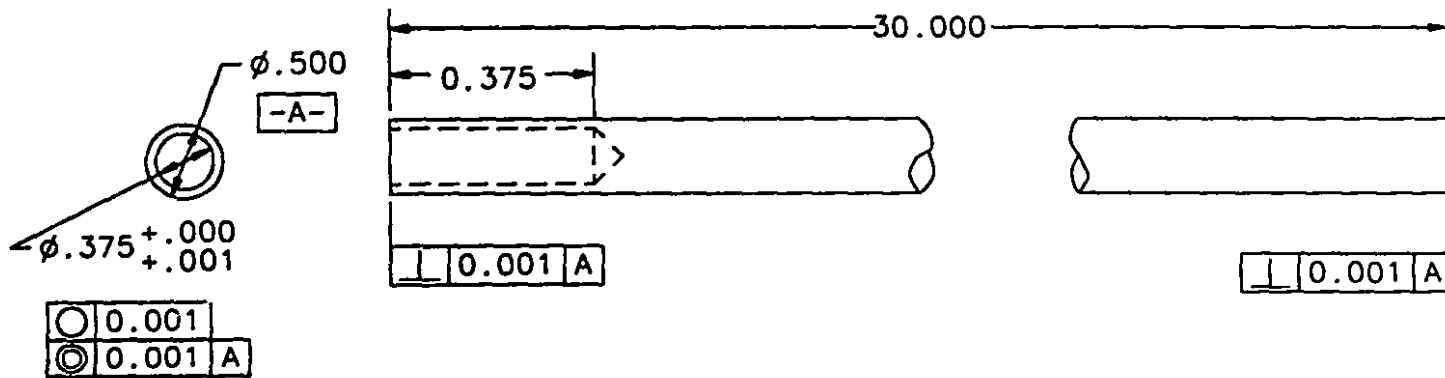
- 1-Material: Tool steel O1
- 2-Bar already ground
- 3-Machine both ends
- 4-Surface roughness to be 53 microinches on both ends



Hopkinson Bars System		McGill University	
Drawing Striker Bar		By Sylvain Riendeau 388-5037	
Scale	Date 4-01-94	General Tolerance ± 0.005	No HBS-01-02 Ver 1

Notes:

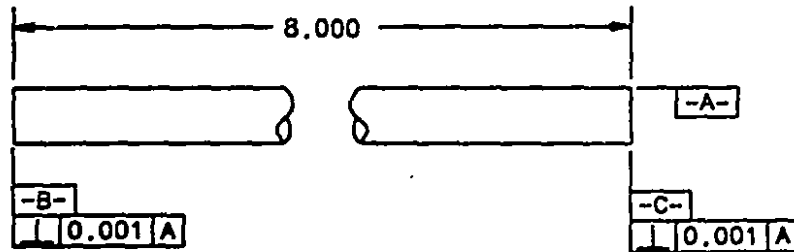
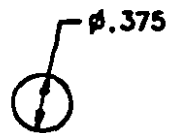
- 1-Material: Tool steel O1
- 2-Bar already ground
- 3-Machine both ends
- 4-Surface roughness to be 53 microinches on both ends



Hopkinson Bars System		McGill University		
Drawing Transmitted		By Sylvain Riendeau 398-5037		
Scale	Date 4-01-94	General Tolerance ± 0.005	No HBS-01-03	Version 1

Notes:

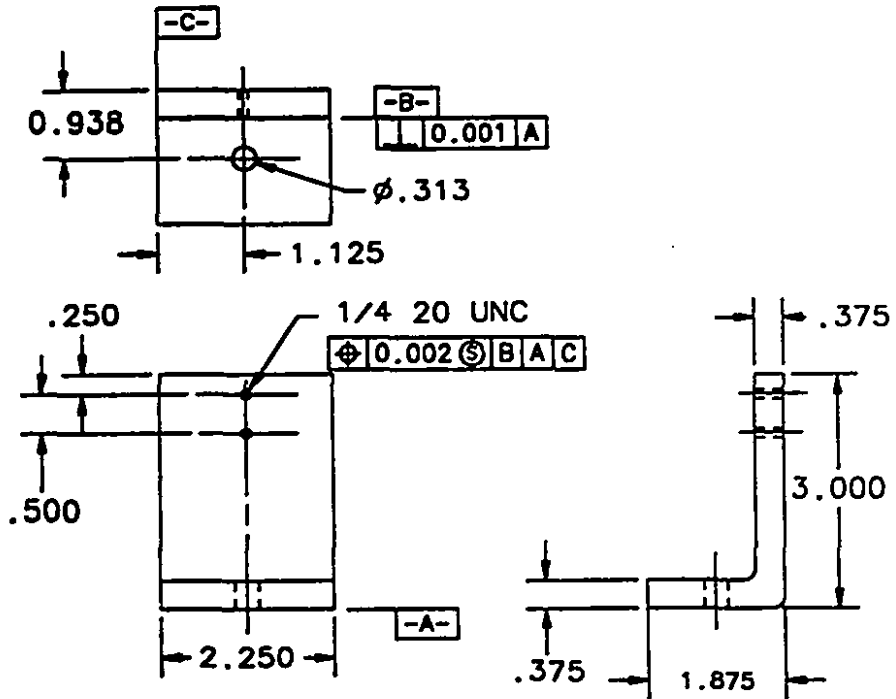
- 1-Material: Tool steel O1
- 2-Bar already ground
- 3-Machine both ends
- 4-Surface roughness to be 53 microinches on both ends



Hopkinson Bars System		McGill University	
Drawing Small striker bar		By Sylvain Riendeau 398-5037	
Scale	Date 4-01-94	General Tolerance ± 0.005	No EBS-01-04 Version 1

Notes:

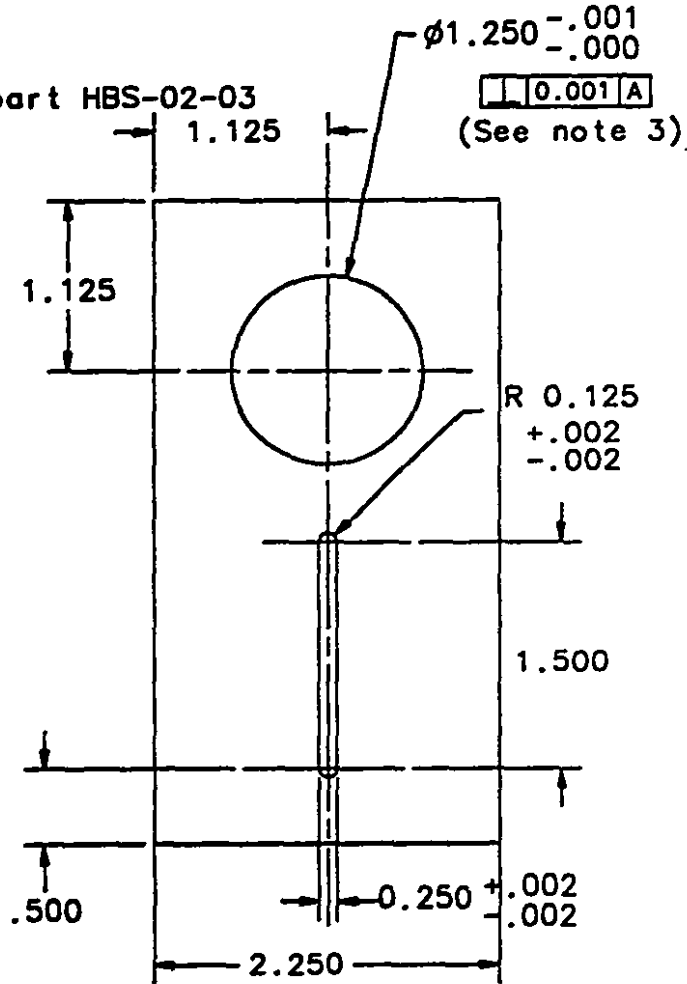
- 1- Material : Steel
- 2- No sharp Edges



Hopkinson Bars System		McGill University	
Drawing Support-L		By Sylvain Riendeau J98-5037	
Scale	Date 17-01-94	General Tolerance ± 0.005	No HBS-02-01 Version 2

Notes:

- 1-Material: Steel
- 2-No sharp edges
- 3-Press fit with part HBS-02-03



\square 0.001 A

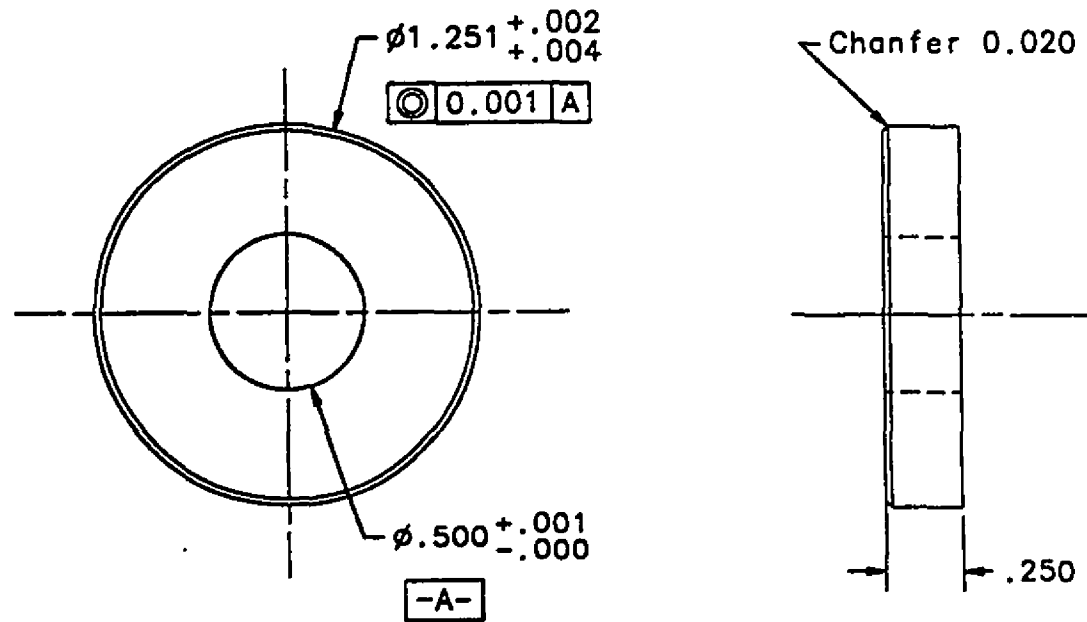
(See note 3)

-A-
 \square 0.001

Hopkinson Bars System		McGill University	
Drawing Support-P		By Sylvain Riendeau 398-5037	
Scale	Date 17-01-94	General Tolerance: 0.005	No HBS-02-02
			Version 2

Notes:

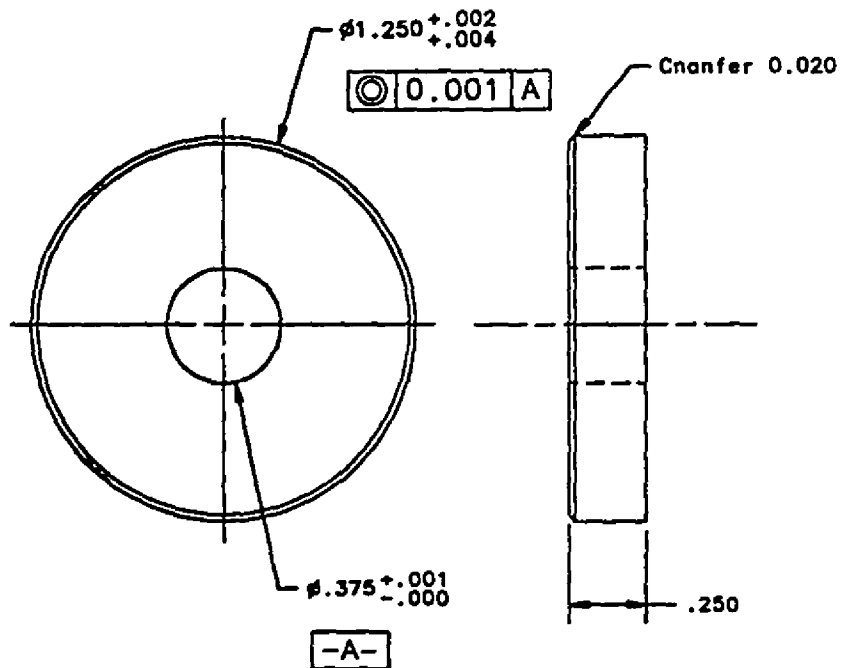
- 1-Material:
- 2-To be press fit with part hbs-02-02



Hopkinson Bars System		McGill University	
Drawing Bushing		By Sylvain Riendeau 398-5037	
Scale	Date 17-1-94	General Tolerance ± 0.005	No HBS-02-03 Verles 1

Notes:

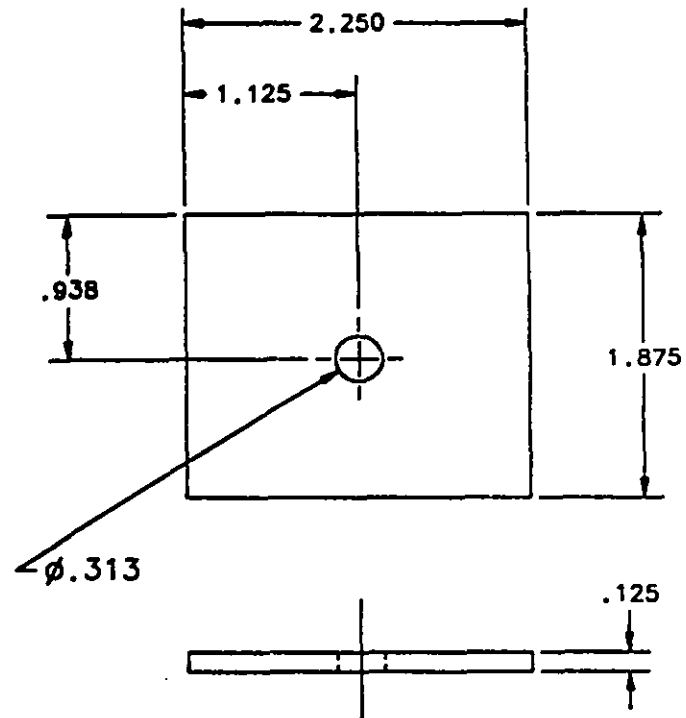
- 1-Material:
- 2-To be press fit with part hbs-02-02



Hopkinson Bars System		McGill University	
Drawing	Bushing-small hole	by	Sylvain Riendeau 398-5037
Scale	Date 18-1-94	General Tolerance	± 0.005
		No	HBS-02-04 Version 1

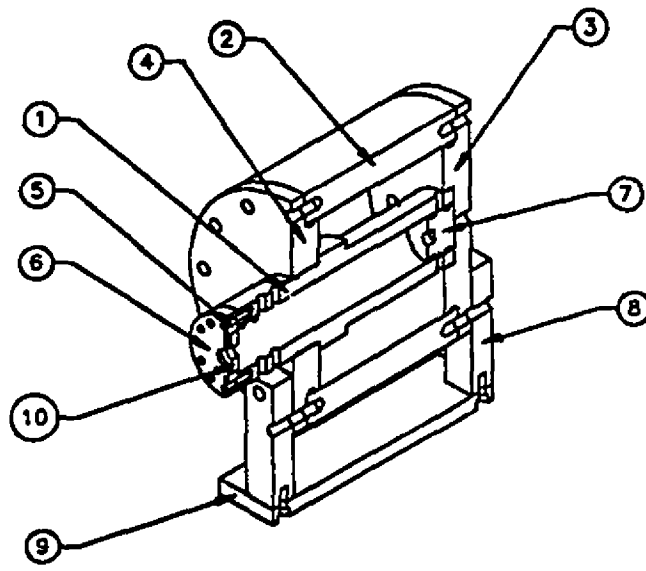
Notes:

1-Material:

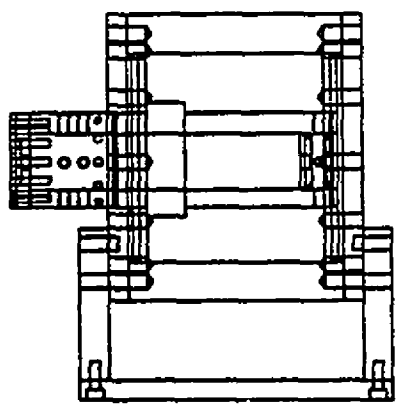


Qty 6

Hopkinson Bars System		McGill University	
Drawing Spacer		By Sylvain Riendeau 308-5037	
Scale	Date 3-2-94	General Tolerance : 0.005	No EBS-02-05 Version 1



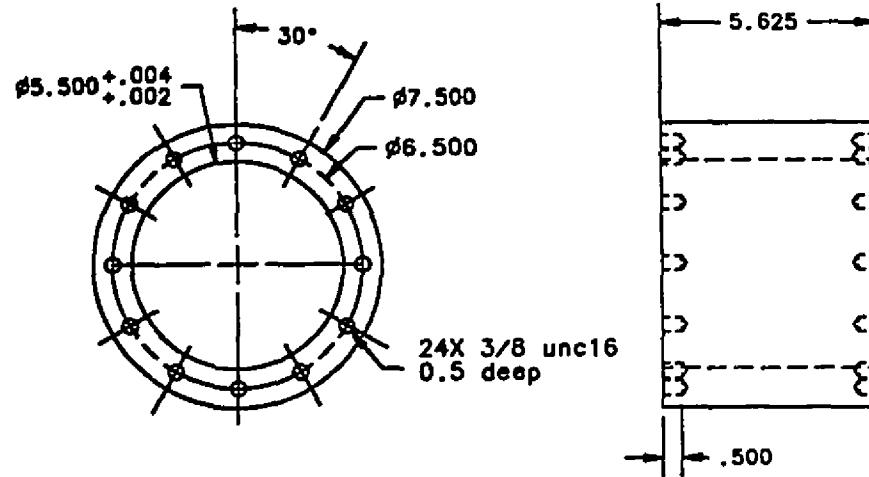
No	Part name	Part number
1	Barrel	HBS-03-01
2	Outer tube	HBS-03-02
3	Back plate	HBS-03-03
4	Front plate	HBS-03-04
5	Stopper disk	HBS-03-05
6	Front sheet	HBS-03-06
7	Sabot	HBS-03-07
8	Leg	HBS-03-08
9	Lower plate	HBS-03-09
10	Bushing	HBS-02-04



Hopkinson Bars System		McGill University	
Drawing GUN ASSEMBLY		By Sylvain Riendeau 398-5037	
Scale	Date 7-03-94	General Tolerance : 0.005	No HBS-03-A1
			Version 1

Notes:

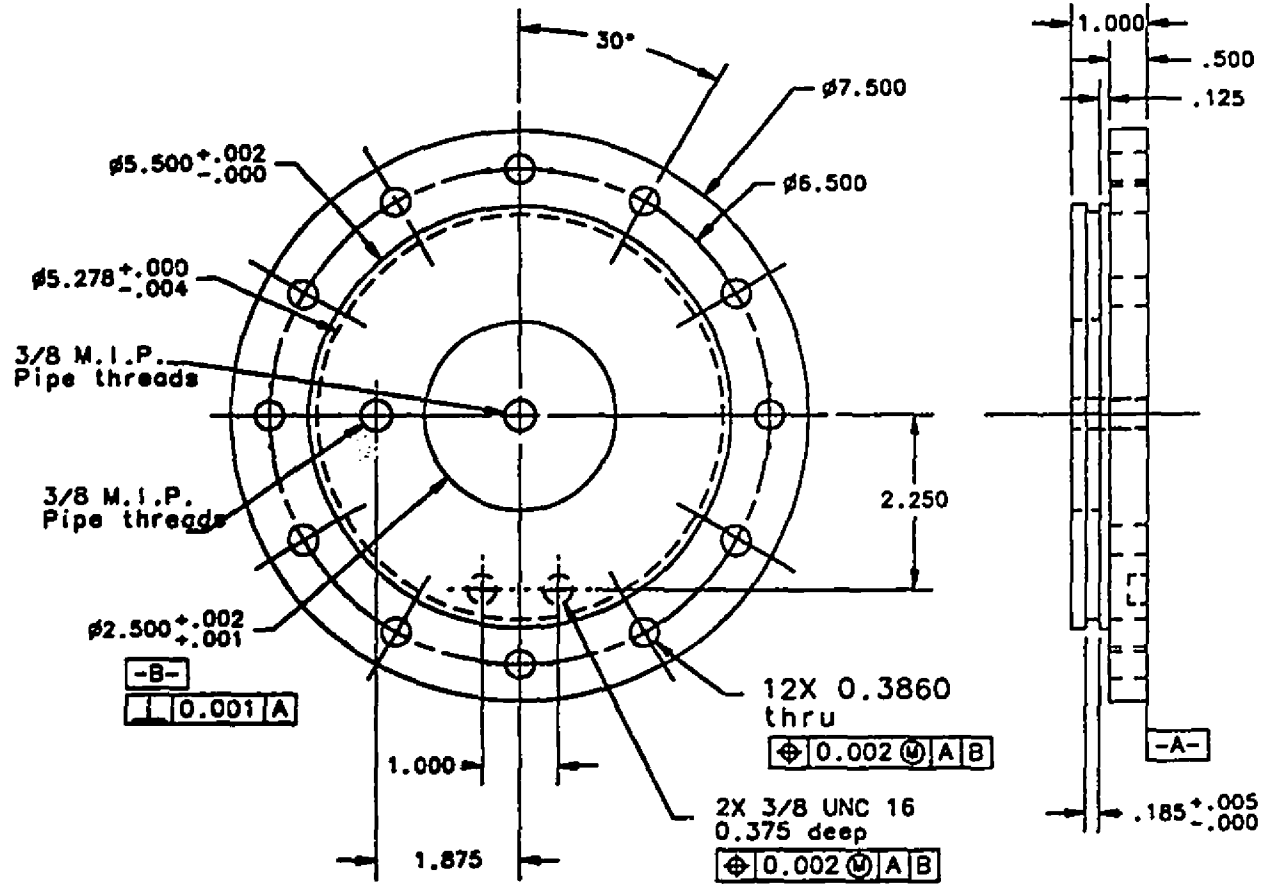
1. Material: Steel
2. Make from supplied tube



Hopkinson Bars System		McGill University	
Drawing Outer tube		By Sylvain Riendeau 398-5037	
Scale	Date 4-3-94	General Tolerance : 0.005	No HBS-03-02
			Version 1

Notes:

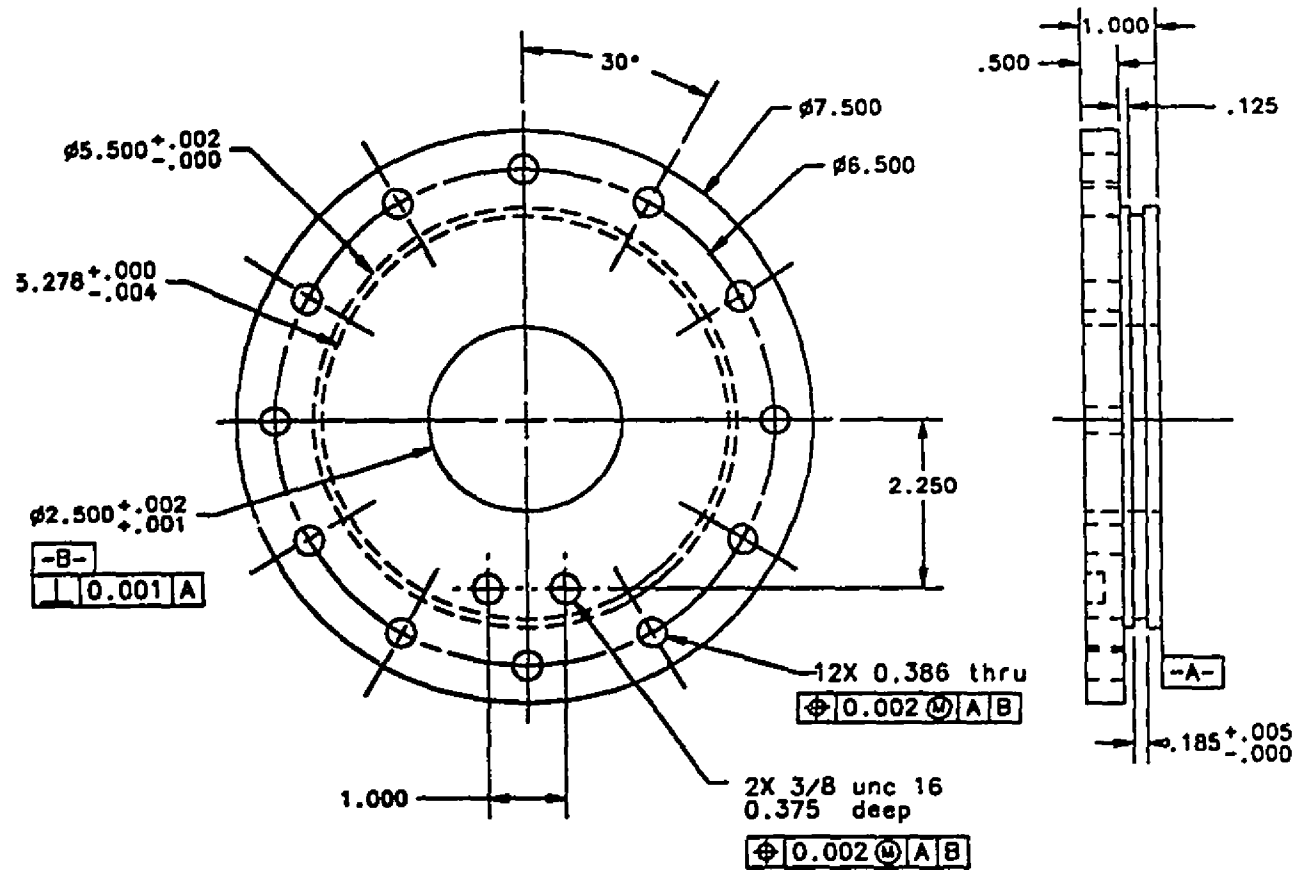
1-Material: steel



Hopkinson Bars System		McGill University	
Drawing Back plate		By Sylvain Riendeau 398-5037	
Scale	Date 9-3-94	General Tolerance ±0.005	No HBS-03-03
			Version 1

Notes:

1-Material: steel

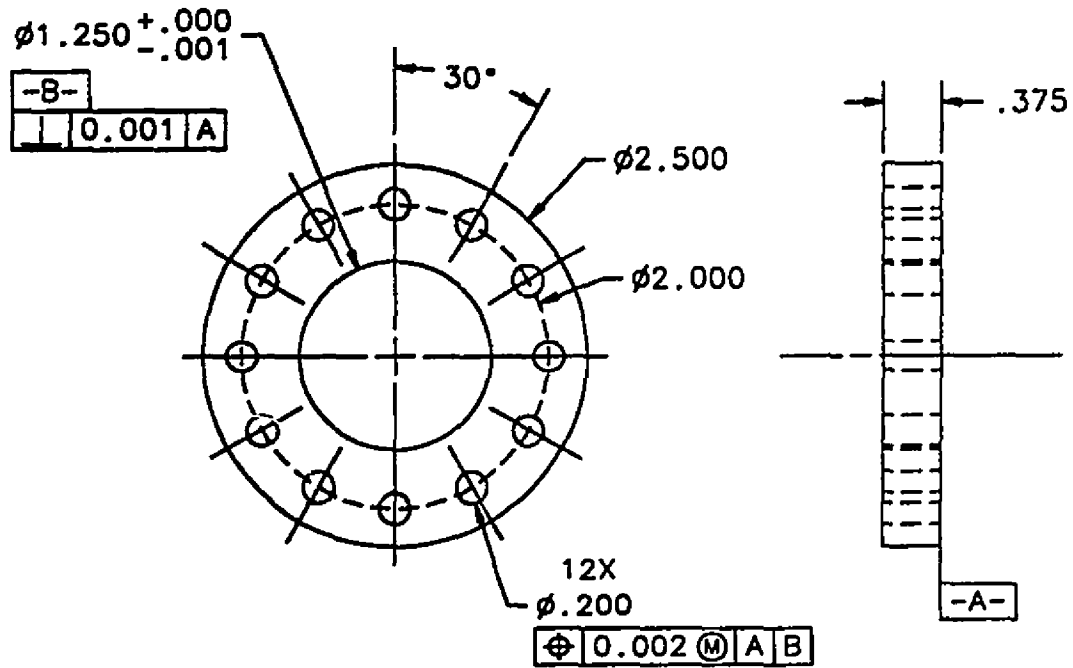


Hopkinson Bars System		McGill University	
Drawing Front plate		By Sylvain Riendeau 398-5037	
Scale	Date 11-3-94	General Tolerance : 0.005	No HBS-03-04
			Version 1

Notes:

1-Material: steel

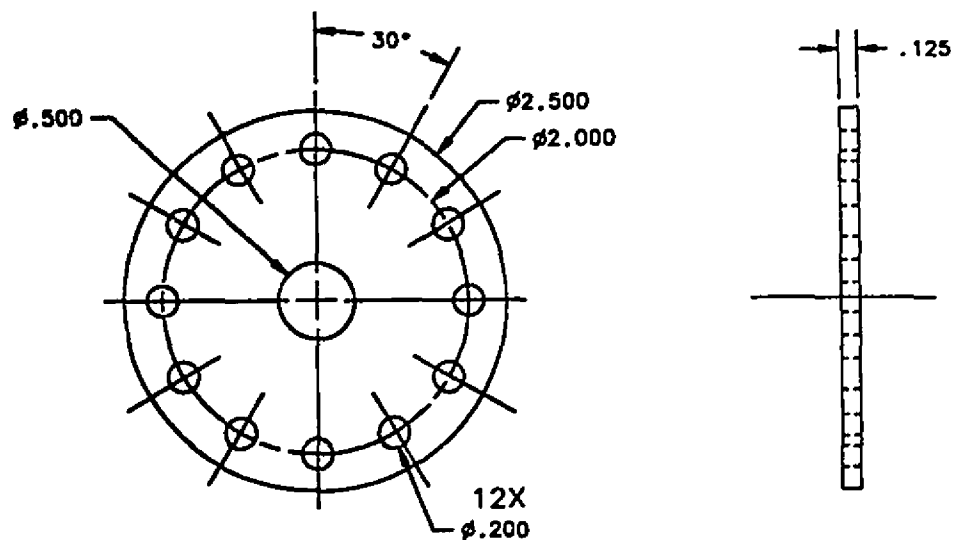
2-To be press fit with part hbs-02-04



Hopkinson Bars System		McGill University	
Drawn	Stopper disk	By	Sylvain Riendeau 398-5037
Scale	Date 14-03-94	General Tolerance	: 0.005
		No	HBS-03-05
		Version	1

Notes:

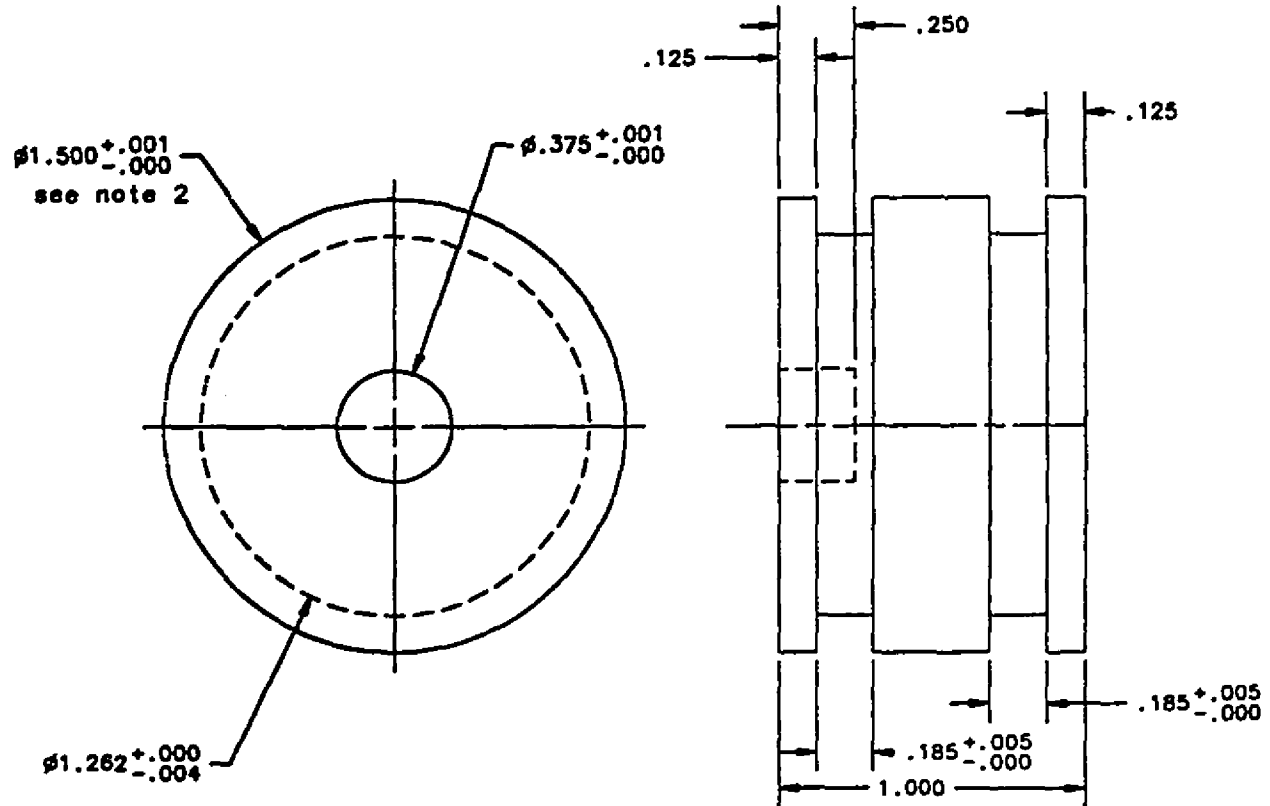
1-Material: steel



Hopkinson Bars System		McGill University	
Drawing	front sheet	By	Sylvain Riendeau 398-5037
Scale	Date 14-03-94	General Tolerance	: 0.005
		No	HBS-03-06
		Version	1

Notes:

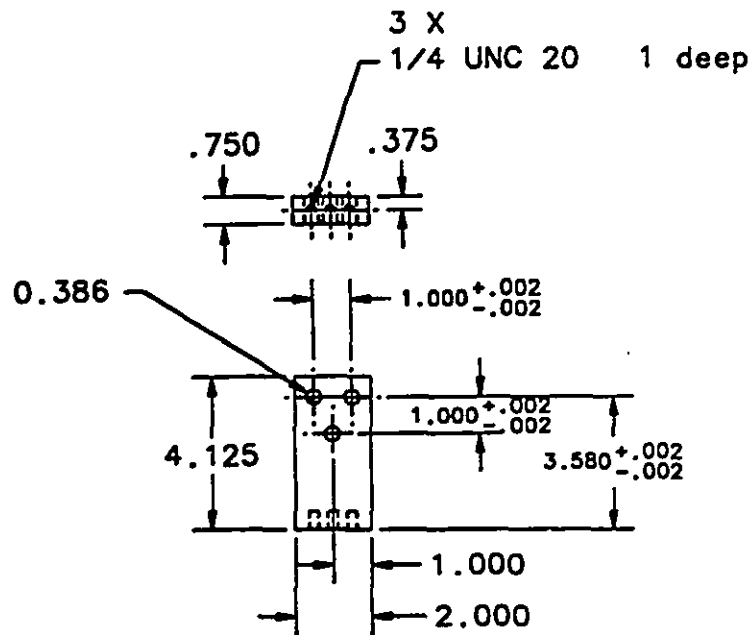
- 1-Material: Delrin
- 2-Slide fit with part hbs-03-01



Hopkinson Bars System			McGill University	
Drawing Sabot			By Sylvain Riendeau 398-5037	
Scale	Date 11-3-94	General Tolerance ± 0.005	No HBS-03-07	Version 1

Notes:

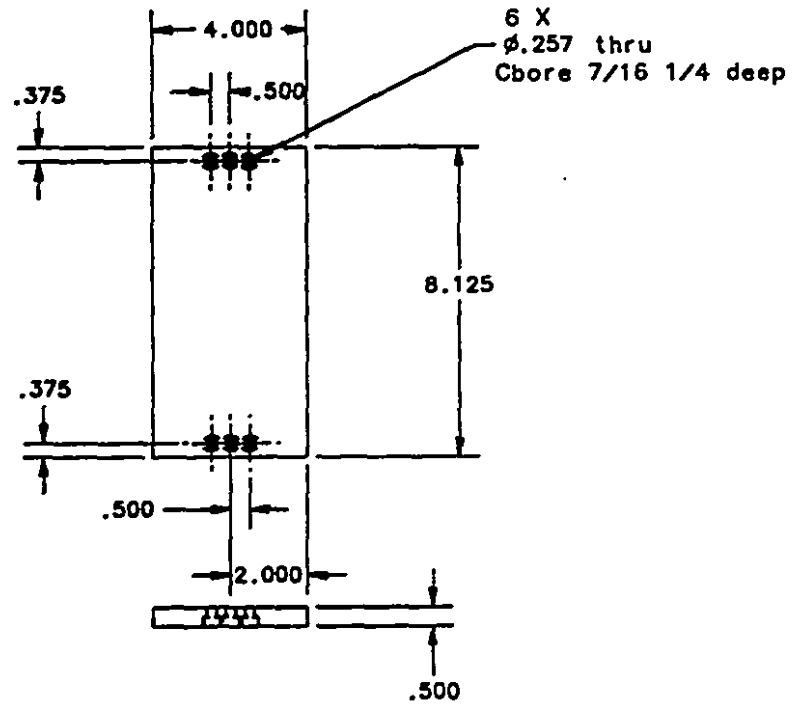
1-Material: steel



Hopkinson Bars System		McGill University	
Drawing Leg		By Sylvain Riendeau 398-5037	
Scale	Date 15-3-94	General Tolerance : 0.005	No HBS-03-08 Version 1

Notes:

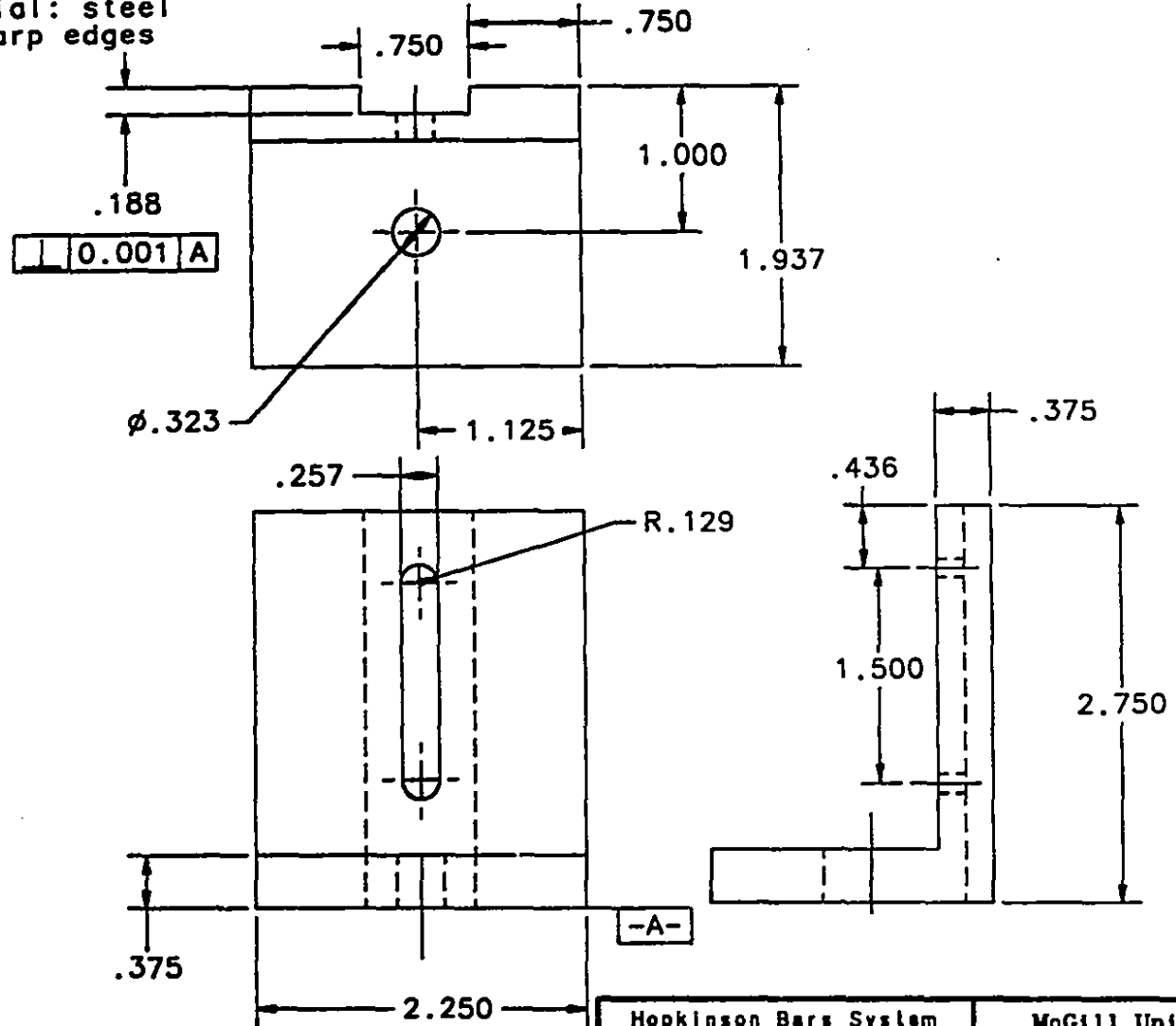
1-Material: steel



Hopkinson Bars System		McGill University	
Drawing	Lower plate	By	Sylvain Riendeau 398-5037
Scale	Date 16-03-94	General Tolerance	: 0.005
		No	HBS-03-09
		Version	1

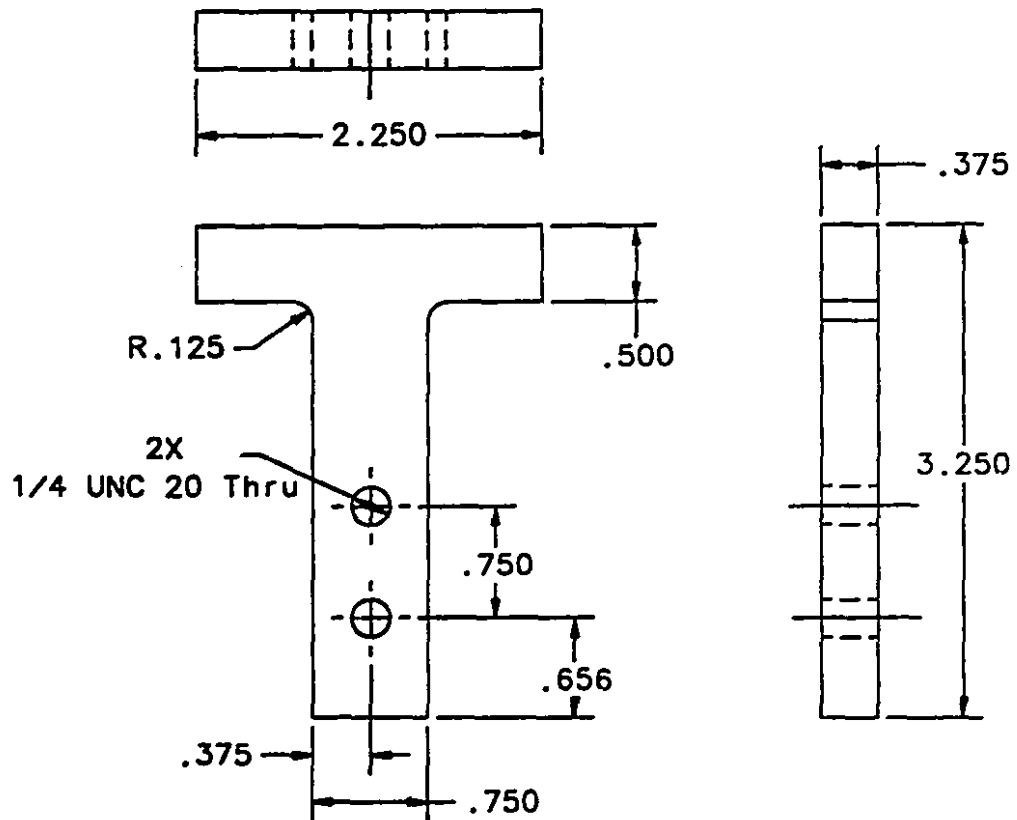
Notes:

- 1- Material: steel
- 2- No sharp edges



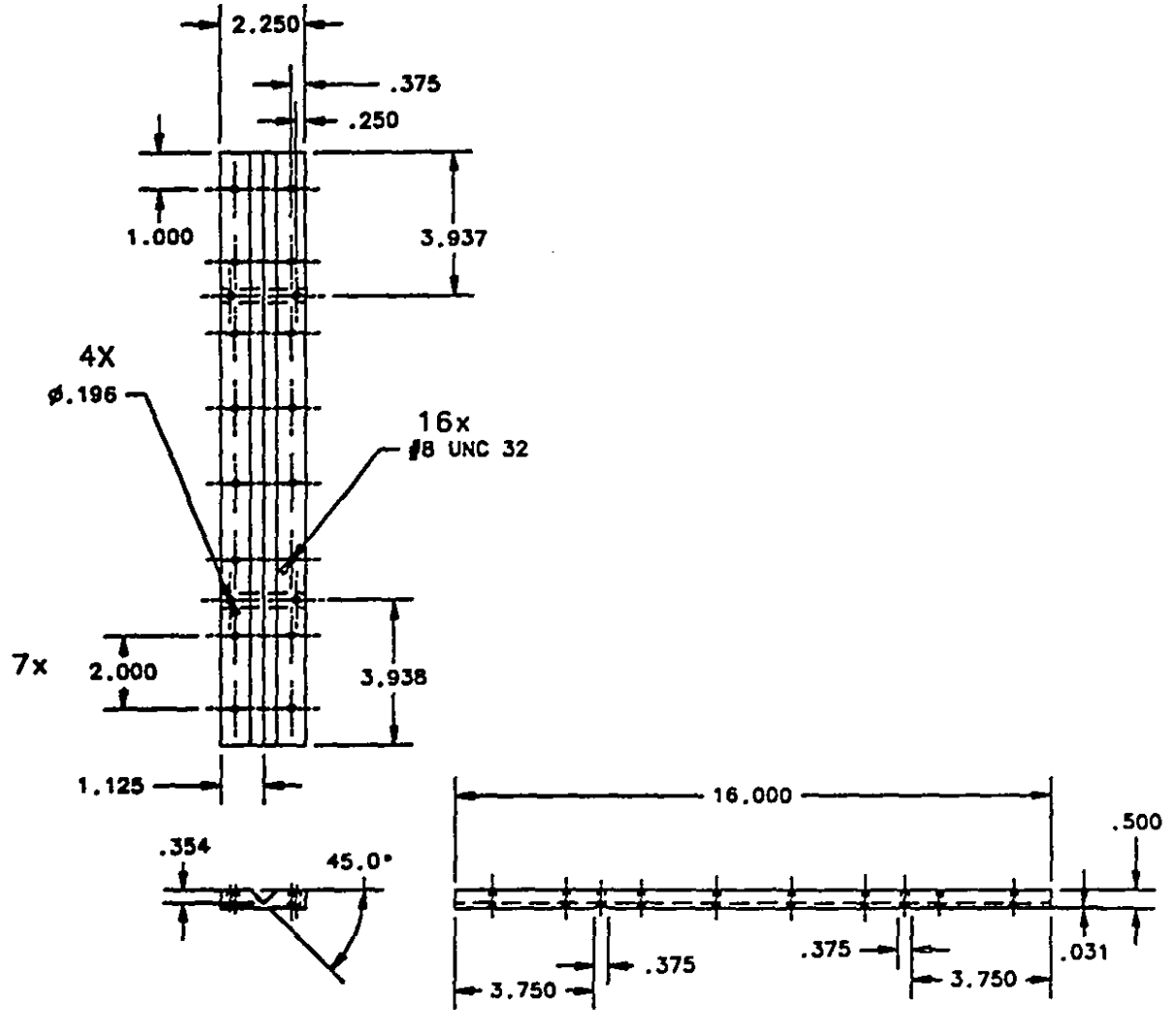
Hopkinson Bars System		McGill University	
Drawing	Slider-L	By	Sylvain Riendeau 398-5037
Scale	Date 26-5-93	General Tolerance	: 0.005
		No	HBS-04-01
		Version	1

Notes:
 Material: Steel
 No sharp edges

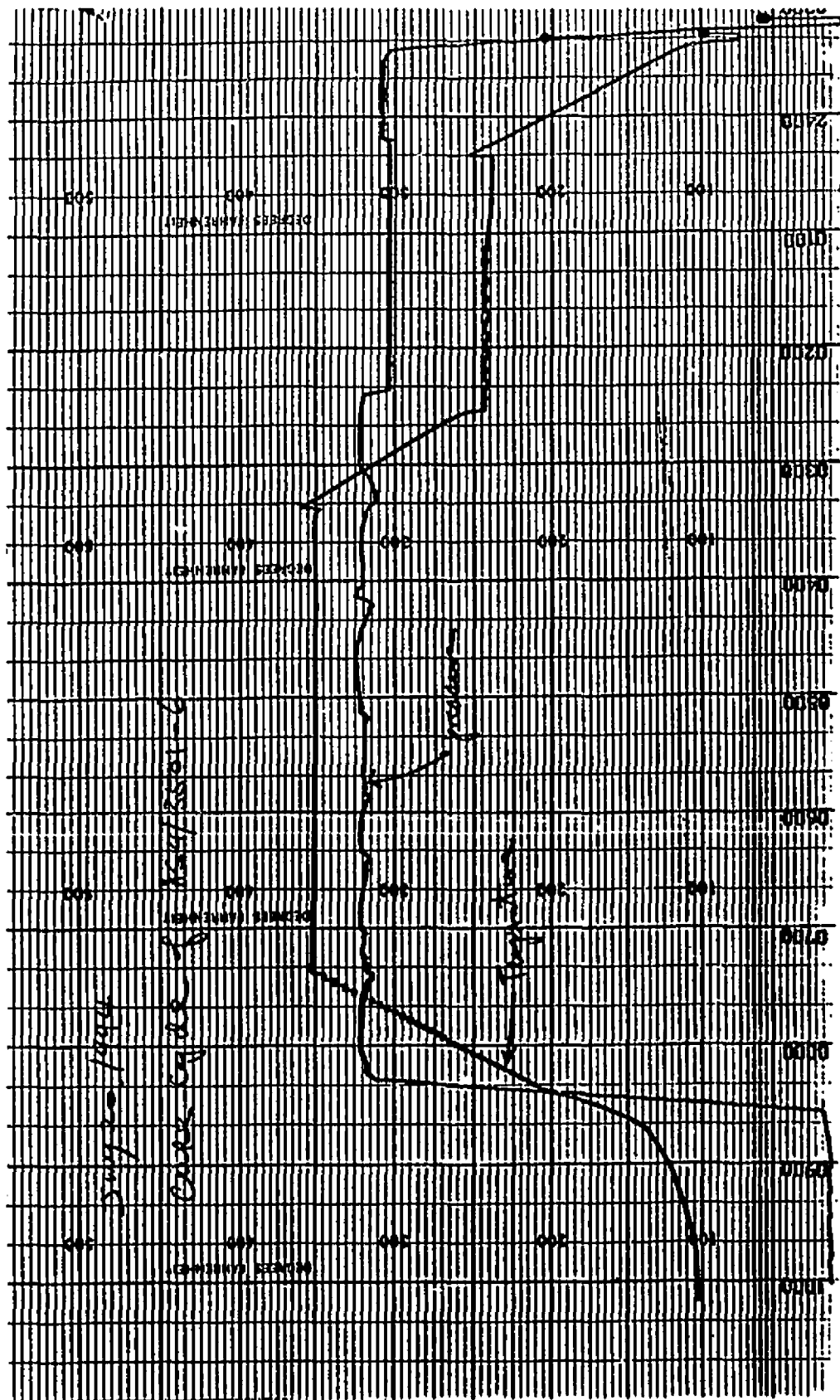


Hopkinson Bars System		McGill University	
Drawing Slide-T		By Sylvain Riendeau 398-9037	
Scale	Date 26-5-94	General Tolerance : 0.005	No EBS-04-02
			Version 1

Notes:
 1-Material: Steel
 2-No sharp edges



Hopkinson Bars System		McGill University	
Drawing Slider plate		By Sylvain Riendeau 398-5037	
Scale	Date 26-5-94	General Tolerance ± 0.005	No BBS-04-03 Version 1



883

884

